Automated Analysis of Intracranial Aneurysm Morphology and Dynamics from CTA Data

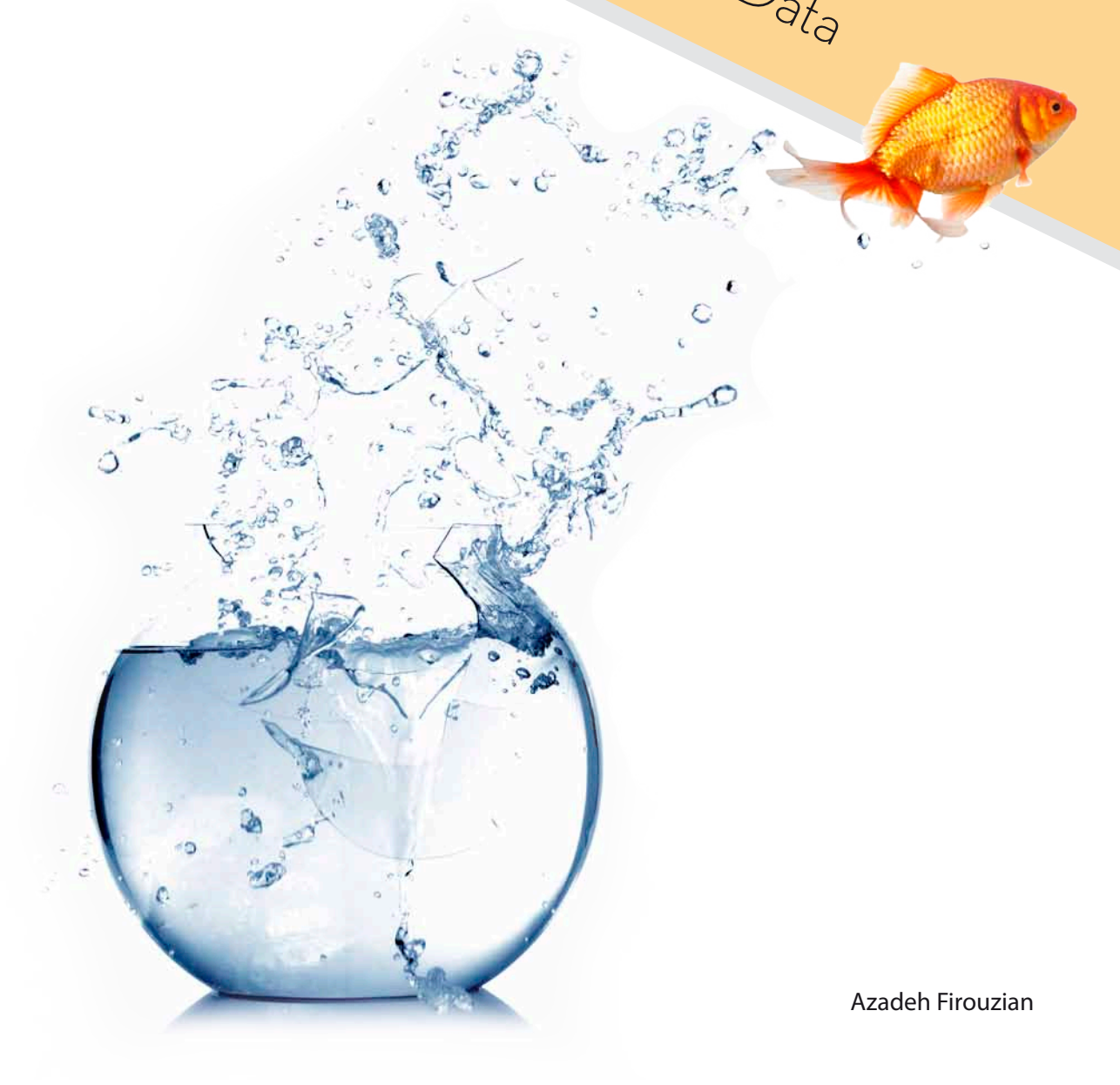

Azadeh Firouzian

Automated Analysis of Intracranial Aneurysm Morphology and Dynamics from CTA Data

Azadeh Firouzian

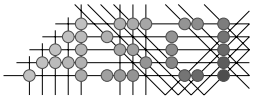

This work was carried out in the ASCI graduate school.
ASCI dissertation series number 267.

The research in this book was conducted at the Departments of Radiology and Medical Informatics of the Erasmus Medical Centre Rotterdam, the Netherlands.

Additional financial support for publishing this thesis was kindly provided by the Department of Radiology of Erasmus MC Rotterdam, the Erasmus University Rotterdam and the ASCI graduate school.

About the cover:
A goldfish jumping out of a broken fishbowl, representing a life threatening explosion; Goldfish is an essential item of the Nowruz (Persian New Year) table and symbolizes life in Iranian mythology. It also represents the month Pisces when the sun is leaving it and spring starts.

ISBN: 978-94-6169-343-3

layout and printing by: Optima Grafische Communicatie, Rotterdam, The Netherlands

Automated Analysis of Intracranial Aneurysm Morphology and Dynamics from CTA Data

Geautomatiseerde analyse van de morfologie en dynamiek van intracraniële aneurysmata uit CTA beelden

Thesis

to obtain the degree of Doctor from the
Erasmus University Rotterdam
by command of the rector magnificus

Prof.dr. H.G. Schmidt

and in accordance with the decision of the Doctorate Board.
The public defense shall be held on
Friday January 25th 2013 at 9:30 am

by

Azadeh Firouzian
born in Tehran, Iran

DOCTORAL COMMITTEE

Promotor:	**Prof. dr. W.J. Niessen**
Other members:	**Prof. dr. D.W.J. Dippel**
	Prof. dr. ir. A.F.W. van der Steen
	Prof. dr. ir. C.H. Slump
Copromotor:	**Dr. ir. R. Manniesing**

Contents

تقدیم به :

پدر و مادر عزیزم

و

خواهر کوچولوم

To:
My dear parents
and
My little sister

درخت تو گر بار دانش بگیرد

به زیر آوری چرخ نیلوفری را

(ناصر خسرو، قرن چهارم و پنجم هجری)

Should your tree bear the fruit of knowledge
You vanquish the azure firmament

(Naser Khosrow, a Persian poet and philosopher)

Chapter 1

Introduction

The worst headache of his life, a sudden onset of severe headache accompanied by nausea, blurred vision, stiff neck and loss of consciousness, happened when he was simply at home doing daily activities. He had no symptoms before it happened and after he was taken to the hospital, he was diagnosed with aneurysmal subarachnoid hemorrhage.

Cerebrovascular diseases, mainly stroke, are the second leading causes of death worldwide according to the WHO. Approximately 5% to 15% of stroke cases have aneurismal origin [1] with a 30-day mortality rate of 45%. Among the survivors 30% has moderate-to-severe disabilities [2]. No less than an estimated 2% of the population has an intracranial aneurysm but fortunately only a few of them rupture, with an annual estimated risk of 0.7% [3]. Research shows that most aneurysms are small and 50% to 80% of them do not rupture during the course of a person's life [4]. Between 10% to 30% of the patients have multiple aneurysms [5].

By definition, intracranial aneurysms are pathological dilations of intracranial arteries and are most commonly located at the branching points of the major arteries passing through the subarachnoid space at the base of the brain, called Circle of Willis (Figure 1). Part of the arterial wall becomes weak and, as a result of blood pressure, starts to grow like a balloon, mostly with an irregular appearance [5]. Little is known about the cause of intracranial aneurysms or the process by which they form, grow and rupture [6]. Subarachnoid hemorrhage (SAH: bleeding in the area surrounding the brain) due to rupture of an intracranial aneurysm is a devastating

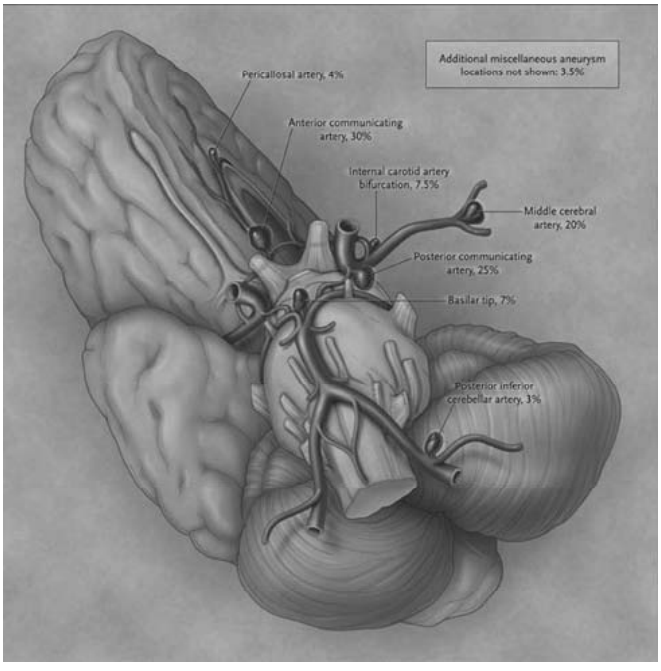

Figure 1. Schematic drawing of the brain, showing the most frequent locations of aneurysms. Percentages indicate the incidence of intracranial aneurysms [4].

event, associated with a high morbidity and mortality rate. Important risk factors of aneurysmal SAH are familial preponderance, hypertension, smoking, alcohol abuse [7], female sex, age [3] and previous aneurysms [5].

Intracranial aneurysms are often referred to as a ticking time bomb since they hardly have any symptoms before they rupture. Most patients are presented to the hospital after rupture or are diagnosed by coincidence. An estimated 10% of the patients die before reaching medical attention [8]. Owing to the increasing availability and improved sensitivity of noninvasive imaging techniques, unruptured aneurysms are increasingly detected. Computed tomography (CT) of the head without contrast material is the initial diagnostic test of choice for suspected SAH [6]. CT angiography (CTA), magnetic resonance angiography (MRA), or angiography by direct intra-arterial catheterization can subsequently be performed for further investigation, e.g. to identify and delineate the size and shape of an intracranial aneurysm. CTA is most widely used in the clinical setting, since it is non-invasive, has high spatial resolution, is faster and cheaper than MRA and can be used for patients who have been treated.

Observation, surgical intervention (clipping) and intravascular intervention (coiling) are three approaches to manage intracranial aneurysms (Figure 2). All ruptured aneurysms are treated, while unruptured ones are managed electively. Several studies suggest that treating aneurysms by coiling is safer than clipping [9,10,11]. Success of aneurysm treatment depends on how far the aneurysmal sac can be excluded from the intracranial circulation while preserving the parent artery. Several factors such as anatomy of the circulation, aneurysm morphology and collateral circulation influence the success rate. Aneurysms with a narrow neck (≤4mm) and small dome size (≤10mm) have the highest success rate. The decision whether to treat the aneurysm or not depends on the estimated rupture risk [12].

Intracranial aneurysms have received considerable attention in recent years and different aspects of this life threatening disease have been investigated. One of the main research questions is to find parameters that could help to predict aneurysms rupture risk. Aneurysm rupture risk has been shown to depend more on aneurysm characteristics than those of the patient.

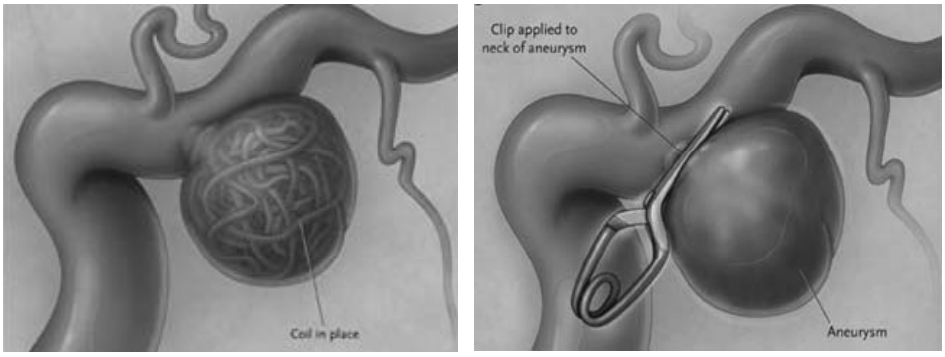

Figure 2. Two methods of aneurysm treatment: coiling (left) and clipping (right) [4]

Size, location and shape have been shown to be associated with rupture risk [12] and assessing these parameters may help in developing a more tailored aneurysm management.

In order to be used in rupture risk assessment, parameters related to aneurysm size and shape need to be accurately and objectively quantified. Size is a well-defined quantitative parameter, which is measured mostly by manual interaction in clinics. Shape characteristics, on the other hand, are more qualitative features, and hence more difficult to quantify. Several studies have been carried out to introduce different shape indices and geometrical analyses using computer algorithms [13,14,15].

Next to aneurysm morphology, their dynamic behavior over the cardiac cycle may provide additional information about their rupture risk. Aneurysmal wall motion has been visualized using ECG-gated CTA [16,17] and it has been hypothesized that points with maximum amplitude of pulsation over the heart cycle constitute potential rupture points [18]. Finally, aneurysm growth over longer time spans (years) has been studied as well. Aneurysm growth was shown to be associated with rupture risk, and therefore patients with a growing aneurysm must be identified and followed up [19,20]. Both studies investigating aneurysm morphodynamics and studies investigating aneurysm growth have so far been based on qualitative or manual assessment. Such assessments are prone to inter- and intra-observer variability and may not be as accurate and reproducible as automated approaches. The research presented in this thesis contains contributions in automated analysis of (i) morphometry, (ii) morphodynamics and (iii) growth of intracranial aneurysms.

ANEURYSM MORPHOMETRY

Aneurysmal volume measurement and shape characterization requires initial segmentation for which a number of methods have been proposed in literature, e.g. for MRA [21] and 3DRA [22] data. For our study, we aim at developing an accurate and robust technique to automatically extract aneurysms from CTA data, as this is the imaging modality most frequently used in daily clinical practice. Aneurysm segmentation in CTA data is a challenging task, owing to the relatively small size of the aneurysm with respect to the image resolution, and the fact that vessel intensities overlap with intensity values of the skull base. Therefore, in **Chapter 2,** a novel semi-automatic method for segmentation of brain aneurysms in CTA data is presented and evaluated. The method is implemented using the level set framework. Image intensity, gradient magnitude and intensity variance are used to construct the speed function that steers the level set towards the boundaries of the aneurysm. Parameters for the speed function are derived from image statistics in a region around a single user-defined seed point. Parameter settings of the method are optimized in a training stage. Using this method, 3D segmentation of the aneurysm and surrounding vasculature is obtained. The method is validated against manual annotations for 15 aneurysms. In addition, the effect of applying various types of smoothing, i.e. Gaussian filtering or nonlinear diffusion using either the regularized Perona & Malik equation or edge enhancing diffusion, as preprocessing step on segmentation accuracy is investigated.

ANEURYSM MORPHODYNAMICS

In **Chapter 3**, we turn our attention towards aneurysm dynamics. As stated previously, aneurysm dynamics may provide additional predictive information on rupture risk, since it is related to the mechanical properties of the aneurysm wall. Several modalities have been used to study aneurysm wall motion, such as cine phase-contrast magnetic resonance angiography (MRA) [23], transcranial Doppler ultrasound [24], time-resolved rotational angiography [25] and ECG-gated computed tomography angiography (CTA) [17,18,26,27,28]. CTA is a suitable technique to evaluate aneurysm morphodynamics as it provides high spatial and temporal resolution within a short scanning time. In addition, CTA is used as a routine modality for diagnosis of vascular diseases [17] and can be relatively easy be extended to a 4D ECG-gated scan. Most of the previous studies on aneurysm morphodynamics are focused on aneurysm visualization, apart from a few studies in which aneurysm morphodynamics was quantified manually [31,32]. However, the small size of intracranial aneurysms, their limited volume change over the cardiac cycle, and the limited signal-to-noise ratio (SNR) in 4D CTA, make manual assessment of aneurysmal dynamic behavior a challenging task. Therefore, in our work the dynamic behavior of the aneurysm over the heart cycle is investigated using automated image analysis techniques. Hereto, a combination of the segmentation method developed in Chapter 2, and 4D registration is used. 4D registration yields a deformation field which describes the local deformation of image structures in all phases. Combining aneurysm segmentation and estimated deformations, the aneurysmal wall deformation is determined. The dynamic behavior of the aneurysm over the cardiac cycle is compared to the dynamic behavior of the adjacent vasculature. Additionally, for validation purposes, the volume change of a skull region as a function of cardiac phase is assessed. The method is also evaluated using simulated 4D CTA series with known deformation.

ANEURYSM GROWTH

In **Chapter 4**, automated assessment of aneurysm growth is investigated. Aneurysm growth over time is another risk factor of aneurysm rupture since enlarging aneurysms are more unstable [32]. Some follow-up studies have been performed to model aneurysm growth and rupture rate [34,35,36,37,38,39]. In other studies, patients with aneurysms after aneurysmal SAH had follow-up imaging with Magnetic Resonance Angiography (MRA) [40,41,42] or Computed Tomography Angiography (CTA) [32,42]. Longitudinal studies provide valuable information on aneurysm growth, formation of new aneurysms and can assist in treatment planning. However, as aneurysm growth is typically small over the time window of interest, it is very difficult to accurately measure it. Size and location have been studied as potential predictors of aneurysm growth. Studies using MRA showed that location is not an important predictor for growth [40,41]. In contrast, size is a very good predictor for growth. Aneurysms with a diameter larger than

8-9 mm have the highest probability of growth and rupture [40,41,42] but this does not imply that small aneurysms do not grow [35,40]. Currently, aneurysm growth over time is mostly evaluated by visual inspection [43]. In **Chapter 4**, methods for automatically determining aneurysm growth in a longitudinal CTA study are developed and evaluated. Two methods are considered. The first method is based on the application of the segmentation method (see Chapter 2) to each time point individually. The second method is an adaption of the method introduced in Chapter 3. By treating a longitudinal series of images as a time series (stack of 3D images), and utilizing groupwise registration in combination with aneurysm segmentation of the first time point scan, aneurysm growth is estimated. This method uses all the information from all follow-up scans simultaneously. The methods are applied to 10 aneurysms and evaluated by comparing results with clinical reports from the hospital. To further investigate possible associations of aneurysm growth with size, location, age and sex, in **Chapter 5** the method developed in Chapter 4 is applied to a larger number of patient data (39 aneurysms). For this study, two expert observers manually interpreted the data as well. Inter-observer variability in assessing growth is assessed, and the automated measurements performed by the method are compared to the manual assessments and to inter-observer variability.

REFERENCES

1. Bederson JB, Awad IA, Wiebers DO, et al. Recommendations for the management of patients with unruptured intracranial aneurysms: a statement for healthcare professionals from the Stroke Council of the American Heart Association. Stroke 2000; 31: 2742-2750.
2. Johnston SC, Selvin S, Gress DR. The burden, trends, and demographics of mortality from subarachnoid hemorrhage. Neurology 1998; 50: 1413-1418.
3. Rinkel GJ, Djibuti M, Algra A, van Gijn J. Prevalence and risk of rupture of intracranial aneurysms: a systematic review. Stroke 1998; 29(1):251-256.
4. Connolly ES, Solomon RA. Management of unruptured aneurysms. In: Le Roux PD, Winn HR, Newell DW, eds. Management of cerebral aneruysms; 2004: 271-285.
5. Schievink WI. Intracranial aneurysms. N Engl J Med 1997; 336(1):28-40.
6. Brisman JL, Song JK, Newell DW. Cerebral aneurysms. N Engl J Med 2006; 355(9):928-939.
7. Feigin VL, Rinkel GJ, Lawes CM, Algra A, Bennett DA, et al. Risk facctors for sunarachnoid hemorrhage: an updated systematic review of epidemiological studies. Stroke 2005; 36(12):2773-2780.
8. Wijdicks EF, Kallames DF, Manno EM, Fulgham JR, Piepgras DG. Subarachnoid hemorrhage: neurointensive care and aneruysm repair. Mayo Clin Proc 2005; 80: 550-559.
9. Jonston SC, Wilson CB, Halbach VV, et al. Endovascular and surgical treatment of unruptured cerebral aneurysms: comparison of risks. Ann Neurol 2000; 48: 11-19.
10. Johnston SC, Zhao S, Dudley RA, Berman MF, Gress DR. Treatment of unruptured cerebral aneurysms in California. Stroke 2001; 32: 597-605.
11. Jonston SC, Dudly RA, Gress DR, Ono L. Surgical and endovascular treatment of unruptured cerebral aneurysms at university hospitals. Neurology 1999; 52: 1799-1805.
12. Dolan JG. Editorial: Clinical decision analysis. Med Decis Making 2001;21:150-151.
13. De Rooij NK, Velthuis BK, Algra A, Rinkel GJ. Confirguration of the circle of Willis, direction of flow, and shape of the aneurysm as risk facctors for rupture of intracranial aneurysms. J Neurol 2009; 256(1):45-50.
14. Millan RD, Dempere-Marco L, Pozo JM, Cebral JR, Frangi AF. Morphological characterization of intracranial aneurysms using 3D moment invariants. IEEE Trans Med Imaging 2007; 26(9):1270-1282.
15. Raghavan ML, Ma B, Harbaugh RE. Quantified aneurysm shape and rupture risk. J Neurosurg 2005; 102(2):355-362.
16. Piccinelli M, Veneziani A, Steinman DA, Remuzzi A, Antiga L. A framework for geometric analysis of vascular structures: application to cerebral aneurysms. IEEE Trans Med Imaging 2009; 28(8):1141-1155.
17. Ishida F, Ogawa H, Simizu T, Kojima T, Taki W. Visualizing the dynamics of cerebral aneurysms with four-dimensional computed tomographic angiography. Neurosurgery 2005; 57(3):460-471.
18. Hayakawa M, Katada K, Anno H, Imizu S, Hayashi J, Irie K, et al. CT angiography with electrocardiographically gated reconstruction for visualizing pulsation of intracranial aneurysms: identification of aneurysmal protuberance presumably associated with wall thinning. AJNR 2005; 26(6):1366-1369.

19. Kato Y, Hayakawa M, Sano H, Suni MV, Imizu S, Yoneda M, et al. Prediction of impending rupture in aneurysms using 4D-CTA: histopathological verification of a real-time minimally invasive tool in unruptured aneurysms. Minim Invasive Neurosurg 2004; 47(3):131-135.

20. Juvela S, Porras M, Heiskanen O. Natural history of unruptured intracranial aneurysms: a long-term follow-up study. J Neurosurg 1993; 79(2):172-182.

21. Law MWK, Chung ACS. Vessel and intracranial aneurysm segmentation using multi-range filters and local variances. MICCAI 2007; 10(Pt 1):866-874.

22. Hernandez M, Frangi AF. Non-parametric geodesic active regions: method and evaluation for cerebral aneurysms segmentation in 3DRA and CTA. Medical Image Analysis 2007; 11(3):224-241.

23. Meyer FB, Huston J 3rd, Riederer SS. Pulsatile increases in aneurysm size determined by cine phase-contrast MR angiography. J Neurosurg 1993; 78: 879-883.

24. Wardlaw JM, Cannon J, Statham PF, et al. Does the size of intracranial aneurysms change with intracranial pressure? Observations based on color "power" transcranial Doppler ultrasound. J Neurosurg 1998; 88:846-850.

25. Zhang C, Villa-Uriol MC, De Craene M, et al. Morphodynamic analysis of cerebral aneurysm pulsation from time-resolved rotational angiography. IEEE Trans Med Imaging 2009; 28:1105-1116.

26. Kato Y, Hayakawa M, Sano H, et al. Prediction of impending rupture in aneurysms using 4D-CTA: Histopathological verification of a real-time minimally invasive tool in unruptured aneurysms. Minim Invasive Neurosurg 2004; 47:131-135.

27. Yaghmai V, Rohany M, Shaibani A, et al. Pulsatility imaging of saccular aneurysm model by 64-slice CT with dynamic multiscan technique. J Vasc Interv Radiol 2007; 18:785-788.

28. Umeda Y, Ishida F, Hamada K, et al. Novel dynamic four-dimensional CT angiography revealing 2-type motions of cerebral arteries. Stroke 2011; 42:815-818.

29. Nishada T, Kinoshita M, Tanaka H, et al. Quantification of cerebral artery motion during the cardiac cycle. AJNR 2011; 32:E206-208.

30. Kuroda J, Kinoshita M, Tanaka H, et al. Cardiac cycle-related volume change in unruptured cerebral aneurysms: a detailed volume quantification study using 4-dimensional CT angiography. Stroke 2012, 43:61-66.

31. Miyazawa N, Akiyama I, Yamagata Z. Risk factors for growth of unruptured intracranial aneurysms: follow-up study by serial 0.5-T magnetic resonance angiography. Neurosurgery 2006; 58(6): 1047-1053.

32. Juvela, S., Poussa, K., Porras, M., "Factors affecting formation and growth of intracranial aneurysms: a long-term follow-up study," Stroke 2001; 32(2): 485-491.

33. Vlak MH, Rinkel GJ, Greebe P, van der Bom JG, Algra A. Trigger factors and their attributable risk for rupture of intracranial aneurysms: a case-crossover study. Stroke 2011; 42(7): 1878-1882.

34. Dickey, P., Kailasnath, P., "The diameter-cube hypothesis: a new biophysical model of aneurysm rupture," Surg Neurol 2002; 58(3-4):166-173.

35. Chang, H. S., "Simulation of the natural history of cerebral aneurysms based on data from the International Study of Unruptured Intracranial Aneurysms," J Neurosurg 2006; 104(2):188-194.

36. Jou, L. D., Mawad, M. E., "Growth rate and rupture rate of unruptured intracranial aneurysms: a population approach," Biomed Eng Online 2009; 18:8-11.

37. Koffijberg, H., Buskens, E., Algra, A., Wermer, M. J., Rinkel, G. J., "Growth rates of intracranial aneurysms: exploring constancy," J Neurosurg 2008; 109(2):176-185.

38. Watton,, P. N., Ventikos, Y., Holzapfel, G. A., "Modeling the growth and stabilization of cerebral aneurysms," Math Med Biol 2009; 133-164.

39. Yoshimoto, Y., "A mathematical model of the natural history of intracranial aneurysms: quantification of the benefit of prophylactic treatment," J Neurosurg 2006; 104(2):195-200.

40. Burns, J. D., Huston, J. 3rd, Layton, K. F., Piepgras, D. G., Brown, R. D., Jr., "Intracranial aneurysm enlargement on serial magnetic resonance angiography: frequency and risk factors," Stroke 2009; 40(2):406-411.

41. Phan, T. G., Huston, J. 3rd, Brown, R. D., Jr., Wiebers, D. O., Piepgras, D. G., "Intracranial saccular aneurysm enlargement determined using serial magnetic resonance angiography," J Neurosurg 2002; 97(5):1023-1028.

42. Sprengers, M. E., van Rooij, W. J., Sluzewski, M., Rinkel, G. J., Velthuizen, B. K., de Kort, G. A., Majoie, C. B., "MR angiography follow-up 5 years after coiling: frequency of new aneurysms and enlargement of untreated aneurysms," AJNR Am J Neuroradiol 2009; 30(2):303-307.

43. Wermer, M. J., van der Schaaf, I. C., Velthuis, B. K., Algra, A., Buskens, E., Rinkel, G. J., "Follow-up screening after subarachnoid haemorrhage: frequency and determinants of new aneurysms and enlargement of existing aneurysms," Brain 2005; 128(Pt 10):2421-2419.

Chapter2

Intracranial Aneurysm Segmentation in 3D CT Angiography: Method and Quantitative Validation with and without Prior Noise Filtering

ABSTRACT

Intracranial aneurysm volume and shape are important factors for predicting rupture risk, for pre-surgical planning and for follow-up studies. To obtain these parameters, manual segmentation can be employed; however, this is a tedious procedure, which is prone to inter- and intra-observer variability. Therefore there is a need for an automated method, which is accurate, reproducible and reliable. This study aims to develop and validate an automated method for segmenting intracranial aneurysms in Computed Tomography Angiography (CTA) data. Also, it is investigated whether prior smoothing improves segmentation robustness and accuracy. The proposed segmentation method is implemented in the level set frame work, more specifically Geodesic Active Surfaces, in which a surface is evolved to capture the aneurysmal wall via an energy minimization approach. The energy term is composed of three different image features, namely; intensity, gradient magnitude and intensity variance. The method requires minimal user interaction, i.e. a single seed point inside the aneurysm needs to be placed, based on which image intensity statistics of the aneurysm are derived and used in defining the energy term. The method has been evaluated on 15 aneurysms in 11 CTA data sets by comparing the results to manual segmentations performed by two expert radiologists. Evaluation measures were Similarity Index, Average Surface Distance and Volume Difference. The results show that the automated aneurysm segmentation method is reproducible, and performs in the range of inter-observer variability in terms of accuracy. Smoothing by nonlinear diffusion with appropriate parameter settings prior to segmentation, slightly improves segmentation accuracy.

This chapter is based on:

Firouzian A, Manniesing R, Flach ZH, Risselada R, van Kooten F, Sturkenboom MC, van der Lugt A, Niessen WJ. Intracranial aneurysm segmentation in 3D CT angiography: method and quantitative validation with and without prior noise filtering, Eur J Radiol 2011; 79(2):299-304.

INTRODUCTION

Intracranial aneurysms are pathological dilations of the major arteries crossing through the subarachnoid space at the base of the brain (Circle of Willis). Intracranial arteries have attenuated tunica media and therefore they are more susceptible to develop an aneurysm compared to extracranial arteries. Aneurysmal rupture, leading to subarachnoid hemorrhage (SAH) is a devastating event and is associated with a high mortality (up to 50%) and morbidity rate [1,2]. Unruptured brain aneurysms do not have indicative symptoms associated and are therefore difficult to diagnose before rupture. Environmental factors such as smoking, hypertension and alcohol consumption are among the risk factors that may lead to aneurysm rupture [3]. A number of studies have reported that aneurysm size is an important risk factor for rupture [4,5,6,7,8,9]. Besides size, the shape of an aneurysm affects its rupture risk [10,11,12,13].

Computed Tomography Angiography (CTA) is widely used in neurovascular imaging as a non-invasive diagnostic tool for detecting and evaluating intracranial aneurysms [14,15]. In clinical practice, automatic quantification of aneurysmal volume and shape parameters may support the pre-operative planning in choosing the right size and type of the first coil. Furthermore, aneurysmal volume measurements are used in determining the packing density, which is a predictor for coil compaction [16,17].

Non-invasive imaging techniques provide the opportunity of screening for unruptured aneurysms and thus pave the way for preventive strategies. Automatic, objective quantification of aneurysmal volume and shape parameters is relevant for predicting rupture risk and for the assessment of small changes in follow-up studies of unruptured aneurysms.

Aneurysmal volume measurement and shape characterization requires initial segmentation for which a number of methods have been proposed in literature. Law et al. developed a method based on multi-range filters and local variances to perform segmentation of intracranial aneurysms on Phase Contrast Magnetic Resonance Angiography (PCMRA) data [18]. Hernandez et al. presented a segmentation method for intracranial aneurysms based on geometric deformable models and applied them to CTA and 3D Rotational Angiography (3DRA) [19] data. In this work they developed a method based on Geometric Active Regions (GAR) which requires training on a number of training data to get statistical information on the intensity.

In this chapter, a novel semi-automatic aneurysm segmentation method based on Geodesic Active Contours (GAC) [20] for segmenting brain aneurysms from 3D CTA is presented and quantitatively evaluated. The method is implemented in the level set frame work. Image intensity, gradient magnitude and intensity variance are used to construct the speed function that steers the level set evolution. Parameters for the speed function are derived from image statistics in a region around a single user-defined seed point. The influence of preprocessing using (nonlinear) smoothing techniques on segmentation accuracy is also evaluated. Three different smoothing techniques are considered, i.e. Gaussian filtering [21], Edge Enhancing Diffusion [22] and regularized Perona-Malik diffusion [23]. Segmentation accuracy is assessed using manual segmentations as reference standard.

MATERIALS AND METHODS

Geodesic Active Contours

The developed semi-automatic method for segmentation of intracranial aneurysms is based on the GAC framework, which was introduced by Caselles et al. [20,24]. In this framework the segmentation is represented by the zero level set of an embedding function. In our case the zero level set represents the aneurysm wall in 3D, i.e. it is a surface in 3D space, and the embedding function is thus a three-dimensional image. By evolving the embedding three-dimensional function in an appropriate way, effectively the 3D surface representing the segmentation is evolved towards the aneurysm boundaries. The evolution of the embedding function Φ can be described by the following Partial Differential Equation (PDE):

$$\Phi_t - \mu \nabla F \nabla \Phi + F(1 - \varepsilon k_{mean}) \left| \nabla \Phi \right| = 0 \quad (1)$$

where F is a speed function derived from the energy term to be minimized and when properly chosen, drives the zero level set towards the aneurysm wall. Furthermore, ε is a weighting factor which determines the influence of the surface smoothness term, k_{mean} is the mean curvature, and μ is the weighting factor of the advection term. The term, εk_{mean} penalizes large deviations of the surface curvature and hence larger values of ε result in smoother surfaces. For aneurysm segmentation the choice of k_{mean} for geometric smoothing is appropriate, as aneurysms generally have a spherical shape, and therefore we would like to have smoothness in all directions (in case of vessel segmentation, k_{min} which is the minimal curvature is to be preferred as it gives smoothness along the longitudinal vessel direction). The level set is initialized with a curve of a certain radius from the seed point. Upon convergence of Equation (1), the resulting zero level set defines the extracted aneurysm surface.

The level set is initialized with a single user defined seed point. This point is used to gather image intensity statistics in the neighborhood of the seed point for defining the image-based speed terms in the speed function and for the fast marching algorithm [24,25] to obtain the initial level set.

Speed Image

As mentioned previously, the speed function is based on three different image-based features. The intensity feature is calculated based on estimates of the aneurysm (g_v) and background (g_b) intensity distributions around the user defined seed point, and are modeled by normal distributions [26]. The size of the neighborhood has been determined considering the size range of aneurysms and in our application was set to 2 voxels in radius. The background intensity distribution parameters are determined from the intensity values between [-200,200] HU; these voxels were considered to constitute the image background. The intensity speed function is then defined as follows:

$$F_i = \frac{g_v - g_b}{g_v + g_b} \tag{2}$$

where F_i denotes the intensity based speed function, and equals zero when the intensity distribution of the aneurysm and background intersect (i.e. it minimizes misclassifications, assuming Gaussian distributions of both vessel and background intensities). F_i approaches -1 for low intensity values, and 1 for high intensity values. The next image feature is a decreasing function of the gradient magnitude:

$$F_{grad} = e^{-\left(\frac{|\nabla I|}{\gamma}\right)^2} \tag{3}$$

where $|\nabla I|$ is the gradient magnitude, γ is a tuning factor. This feature slows down the zero level set near edges by assigning a low value to the speed image when there is a high gradient value.

Local intensity variance is the third feature that is included in the speed function. As the intensity inside the vessels in CTA is assumed to be homogeneous, a lower intensity variance is to be expected within the aneurysm. Using this assumption and considering that we would like our speed image to be zero when there is a high variance and 1 when there is none, the speed image is formulated as follows:

$$F_n = e^{-\left(\frac{\sigma}{\beta}\right)^2} \tag{4}$$

where σ is the local standard deviation and β is a tuning factor.

The final speed image combines the three speed terms, as follows:

$$F = F_i . F_{grad} . F_n \tag{5}$$

Owing to the definition of the individual speed terms, the speed function ranges between -1 and 1.

Data Acquisition

Eleven patients were randomly selected from a single-center observational study of a prospectively collected cohort of patients with subarachnoid hemorrhage (SAH) caused by an intracranial aneurysm. In this center CTA was the part of the standard work-up of patients with SAH. Inclusion criteria for the cohort were: 1) clinical diagnosis of non-traumatic subarachnoid hemorrhage,

confirmed by CT or CSF spectrophotometric analysis, 2) age 18 years or over, 3) written informed consent by the patient or relative to review the patient's clinical record and imaging data, 4) intracranial aneurysm on CTA. The protocol was approved by the Institutional Review Board.

CTA image acquisition was performed on a 16-detector row CT scanner (Somatom X-32 Sensation 16; Siemens Medical Solutions, Erlangen, Germany). The scan volume started from the upper limit of the posterior arch of the atlas and extended cephaled with coverage of 100 mm. Eighty ml contrast material (Iodixanol 320 mg/ml – Visipaque – Amersham Health, Little Chalfont, UK) was injected using a power injector (EnVision – MedRAD, Pittsburgh, PN, USA) through an 18-20G iv cannula (depending on the size of the vein), in an antecubital vein with an injection rate of 4 ml/sec. For both the anterior and the posterior circulation 1 mm images with 0.6 mm overlap were reconstructed with a FOV of 100 mm.

Image smoothing

In order to investigate whether prior (nonlinear) diffusion improves segmentation accuracy, three different diffusion filters were applied to the data sets, i.e. Gaussian filtering [21], Edge Enhancing Diffusion (EED) [22] and Regularized Perona-Malik (RPM) [23] diffusion. These filters and relevant parameters are briefly described below:

Gaussian Filtering: The first preprocessing filter is smoothing the image with a Gaussian kernel:

$$u = u_0 * G_\sigma \tag{6}$$

which is equivalent to solving the linear diffusion equation:

$$\partial_t u = div(\nabla u) \tag{7}$$

with $\sigma = \sqrt{2t}$.

Perona-Malik: Perona-Malik is a non-linear diffusion method where the local smoothing depends on the local image gradient magnitude. This smoothing method preserves the edges i.e. it varies the degree of smoothing such that limited smoothing on edges occurs:

$$\partial_t u = div(g(|\nabla u|^2)\nabla u) \tag{8}$$

in which $g(|\nabla u|^2)$ is the edge dependent conductivity. In our implementation the diffusivity is defined as:

$$g(s^2) = \frac{1}{1 + s^2/\lambda^2} \qquad (\lambda > 0) \tag{9}$$

where λ is a tuning parameter.

In the experiments, we used regularized Perona-Malik (RPM) in which the gradient magnitude within the diffusivity is calculated at a certain scale using Gaussian derivatives [27]:

$$\partial_t u = div(g(|\nabla u_\sigma|^2)\nabla u) \tag{10}$$

Edge Enhancing Diffusion (EED): EED is a nonlinear diffusion scheme which smoothes the image considering the gradient magnitude and its orientation:

$$\partial_t u = div(D(\nabla u_\sigma)\nabla u) \tag{11}$$

where D is chosen in a way that smoothing is performed along the edges rather than across the edges and constructed from eigenvectors ($v_1 \parallel \nabla u_\sigma$; $v_2 \perp \nabla u_\sigma$; $v_3 \perp \nabla u_\sigma$ and $v_2 \perp v_3$) and corresponding eigenvalues:

$$\lambda_1 = D(|\nabla u_\sigma|^2) \;;\; D(s^2) = 1 - \exp\left(\frac{-C}{(s/\lambda)^8}\right); \lambda_2 = D(0) = 1 \;; \lambda_3 = D(0) = 1 \tag{12}$$

Evaluation

Three different evaluation measures have been used for this study:

- *Similarity Index (SI)* or Dice score, which is the amount of overlap between the automatic and manual segmentation; it has a value between 0 and 1:

$$\mathrm{SI} = 2\,\frac{|S_{Auto} \cap S_{Man}|}{|S_{Auto}| + |S_{Man}|} \tag{13}$$

  where S_{Auto} represents automatic segmentation and S_{Man} represents manual segmentation.

- *Average Surface Distance (ASD)*, which is the average distance between two segmentation surfaces and is calculated as follows:

$$\mathrm{ASD} = 2h\,(V_{MS} - V_{AS})/\,[(D_{MS} - V_{MS}) + (V_{MS} - E_{MS})] \tag{14}$$

where V_{MS} is the volume of the manual segmentation, V_{AS} is the volume of the automatic segmentation; D_{MS} is the volume of the manual segmentation dilated with 1 voxel and E_{MS} is the volume of the manual segmentation eroded with 1 voxel and h is the voxel size (isotropic).

- *Volume Difference (VD)*, which is the difference in volume of the manual and automatic segmentation of the aneurysm.

Experiments

Our implementation was based on the GAC module provided by the Insight Toolkit (ITK) [28] framework which is a standard forward Euler discretization scheme for the numerical approximation matrix. It has been applied to 15 aneurysms in CTA data sets from 11 patients.

The data sets were divided into a training (10 aneurysms) and a test set (5 aneurysms). Most of the parameter settings involved in the segmentation were not critical and were fixed after pilot experiments: the number of iterations (2000), maximum RMS error which determines the stop criteria of evolution (0.001), radius of the level set at initialization (2 pixel sizes; 0.6 mm), radius of the neighborhood around the seed point to estimate vessel intensity distribution (2 pixels sizes), scale of gradient (1 pixel size; 0.3 mm) and the radius at which the standard deviation is calculated (2 pixel sizes). The curvature scaling and the tuning parameters for the intensity variance and gradient magnitude speed images are the three parameters that need optimization. The curvature scaling (ε in Equation (1)) which smoothes the final segmentation result was varied in the range of [0, 0.1] mm^{-1}. The gradient tuning parameter (γ in Equation (3)) was varied in the range of [10,400] and noise tuning parameter (β in Equation (4)) was varied in the range of [10,200]. These parameters ranges were determined after a first pilot study.

All the experiments were performed on cropped data sets to save calculation time and memory usage. A region of interest (ROI) of 3x3x3 cm^3, which is a good representative of the targeted region for segmentation, was selected around the user defined seed point. To prevent

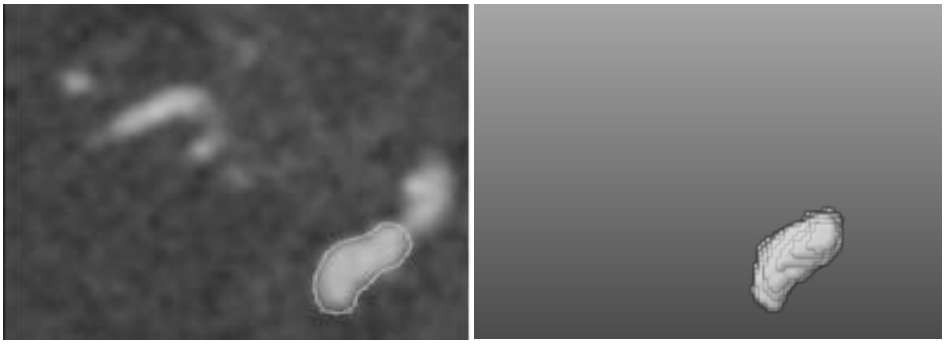

Figure 1. Manually drawn contours around the dome of an aneurysm (located in the Posterior Communicating Artery) on a slice of a 3D CTA data set in an axial view (left); The 3D volume rendering of the binary mask created from the contours which is used in the evaluation section (right). As the contours are made slice by slice, the resulting volume is not smooth.

Figure 2. Volume rendering of an automatic segmentation result (left) and aneurysm (right) separated from surrounding vessels (middle) for evaluation purposes. This aneurysm is located on the posterior communicating artery on the right side.

the voxelized representation from giving large errors in small sized aneurysms, we up-sampled the CTA data prior to automatic segmentations with a factor 2. For the evaluation process, the automatic segmentations were down-sampled back to their original voxel sizes.

For quantitative evaluation, two expert radiologists manually segmented 15 aneurysms in 11 patients using a tool in MeVisLab [29]. After selection of the ROI, the radiologists drew contours around the aneurysm, slice by slice. These contours were defined by the coordinates of the points clicked by radiologists around the aneurysms and converted to a binary mask (Figure 1).

The manual segmentations of one observer (A) were selected as reference, and were used for training and testing of the method. The manual segmentations of the second observer (B) were used for testing the method, and to determine the inter-observer variability. The three parameters (curvature scaling, gradient tuning and noise tuning) were optimized on the training set i.e. SI, ASD and VD were calculated for all the settings and the one with the best result was selected. Manual annotations only cover the aneurysm whereas the automatic segmentations include the aneurysm and the surrounding vessels. For evaluation purposes, the aneurysm in the automatic segmentation was therefore separated from the surrounding vessels using dilation (by 2 voxels) of the manual segmentation as mask (Figure2). Using this mask over the automatic segmentation, it was divided into two parts; one containing the aneurysm and the other one containing the rest of the vessels. The part including the vessels is dilated 2 voxels with the condition that it limits itself to the borders of the original segmentation. This condition is applied to prevent the dilation procedure to eat up small aneurysms. The dilation is applied to compensate for the part of the parent vessel which was cut by the manual mask. The resulting vessel image is subtracted from the original segmentation to get only the aneurysm out.

In the second set of experiments, the effect of pre-filtering on the segmentation results was investigated. The segmentation parameters were set to the optimal values obtained in the first set of experiments. The effect of different smoothing techniques was evaluated for different diffusion times. To make a fair comparison, results were compared at corresponding evolution times (t). The following parameter settings were used for the filters:

Table 1. Evaluation results of the segmentation method with respect to three different evaluation measures. The results are averaged over all data sets.

	Method versus Observer A			Method versus Observer B	Inter-observer
	Training	**Testing**	**Overall**	**Overall**	**Overall**
SI	0.823	0.837	0.828	0.813	0.811
ASD (mm)	0.132	0.121	0.129	0.145	0.162
VD (mm³)	13.397	9.902	12.232	16.117	12.116

- **Gaussian Filtering:** This smoothing technique has one parameter to be set and that is the standard deviation of the Gaussian function (σ), which is directly related to the evolution time. The experiments were performed with Gaussian functions of various standard deviations in the range of [0.15, 2] mm.
- **RPM:** This filter has four parameters to be set. The scale at which the gradient was computed was set to the voxel size (0.3 mm), the weighting factor for the gradient (λ) was set to 100, the time step (Δt) to 0.01, and the number of iterations (n) was calculated according to the scale of the Gaussian filter ($n=\frac{\sigma^2}{2\cdot\Delta t}$). The evolution time can be calculated as $t = n \cdot \Delta t$.
- **EED:** Similar to RPM, the scale of gradient was set at the voxel size (0.3 mm), the contrast parameter (λ) was set to 100, the time step was fixed at 0.01 and number of iterations was calculated in the same way as in RPM.

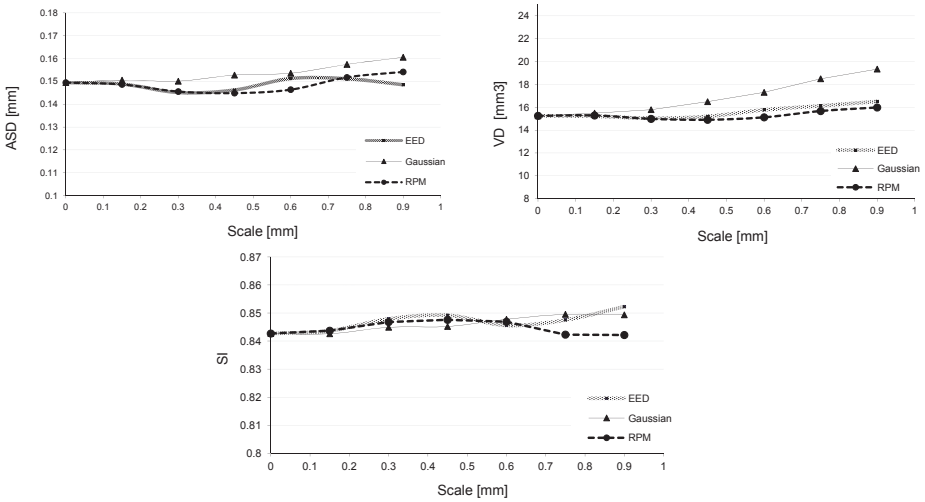

Figure 3. Average SI, VD and ASD over all patients is shown as a function of "equalized" evolution time for Gaussian, EED and RPM diffusion. Scale refers to the scale parameter of Gaussian blurring. For the purpose of comparison EED and RPM have been synchronized using corresponding evolution times.

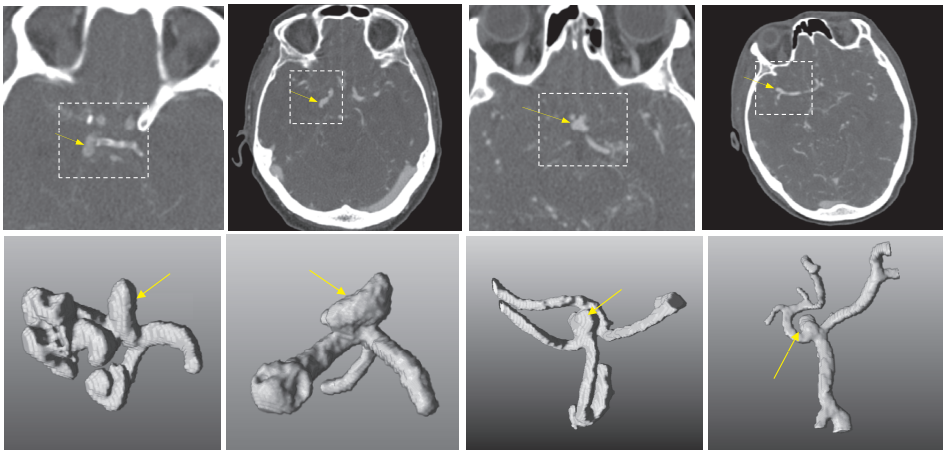

Figure 4. Four examples of segmentation results are shown in the figure. The top row shows the original CTA images on which the ROIs are marked and the bottom row shows the corresponding segmentation results. Arrows indicate the location of the aneurysm. From left to right, the first two aneurysms are located on the right posterior communicating artery, the third aneurysm is located on the left anterior communicating artery and the last one is located on the right middle cerebral artery. A post-processing step is required to separate the aneurysm from both the vasculature and bone. In the first case from the left, the vasculature adjacent to the aneurysm grew into bone which can cause complications in the evaluation process.

RESULTS

The average volume of the 15 aneurysms included in the study was 70.1 ± 69 mm^3. After optimizing the segmentation parameters on the training set, we evaluated the method on the remaining set of aneurysms. The results of training, testing, overall experiments and the inter-observer variability with respect to the three evaluation measures are reported in Table 1. It can be observed that the SI between the automated method and both observer A and B is large, and in the range of the inter-observer variability. Also the average surface distance and volume difference between the method and observers is clearly within the range and often smaller than the inter-observer variability. It can also be observed that performance of the method on the training set is similar as on the test set, indicating that the method is not over-trained.

The influence of prior diffusion filtering on the performance of the segmentation method is shown in Figure3. It can be observed that nonlinear smoothing (EED, RPM) slightly improves segmentation accuracy for small evolution times and that at larger evolution time accuracy decreases.

DISCUSSION

Morphological characterization of intracranial aneurysms is important as volume and shape characteristics have been shown to be associated with rupture risk. For investigating intracranial aneurysms, CTA is the most widely used imaging modality. Segmentation in CTA data is a challenging task, owing to the sometimes relatively small size of the aneurysm with respect to the image resolution, and the fact that vessel intensities overlap with intensity values in the skull base.

A novel semi-automatic level set based segmentation method for brain aneurysms in CTA, which uses image intensity, image gradient and intensity variance, has been developed. A quantitative evaluation study on 15 aneurysms was conducted. The evaluation showed that preprocessing using nonlinear smoothing techniques prior to segmentation slightly improves segmentation accuracy. This has been shown previously as well for 3DRA [30]. In addition, it was shown that the accuracy of the method was in the range of the inter-observer variability. Therefore, the method can be used to replace the tedious procedure of manual outlining. Also, we hypothesize that in longitudinal studies, the use of automated segmentation is potentially better suited to pick up subtle changes in aneurysm volume and shape. This hypothesis is subject of further research.

The method still has some limitations. Firstly, in the current study we focused on the accuracy to determine the volume of the aneurysm. However, our segmentation approach will segment both the aneurysm and surrounding vasculature (Figure4). In order to determine the accuracy with which the aneurysmal wall has been found, we therefore used a ROI defined by the manual reference standard. Recently, a method has been developed [31] which allows the separation of aneurysms from the adjacent vessels with minimum user interaction. Secondly, in four cases, when the aneurysm and its surrounding vessels were very close to the skull base, the segmentation grew into the bone (Figure4). This problem can also be circumvented by separating the aneurysm from the adjacent vessels. However, this separation step is slightly more complex as both the adjacent vessels and bone need to be removed.

CONCLUSIONS

A novel semi-automatic method for segmentation of brain aneurysms in CTA has been developed. The method performs in the range of the inter-observer variability therefore it is accurate and reproducible and has the potential to replace the manual segmentation. Furthermore, we have found that applying nonlinear diffusion prior to segmentation slightly improves segmentation accuracy.

REFERENCES

1. Huang J, van Gelder JM. The probability of sudden death from rupture of intracranial aneurysms: Ameta-analysis. J. Neurosurg 2002; 51(5):1101–1105.
2. Brisman J, Song J, Newell D. Medical Progress: Cerebral Aneurysms. New Eng. J. Med 2006; 355(9):928-939.
3. Schievink WI. Intracranial Aneurysms. N Engl J Med 1997; 336(1):28-40.
4. Beck J, Rohde S, Berkefeld J, et al. Size and location of ruptured and unruptured intracranial aneurysms measured by 3D rotational angiography. Surgical Neurology 2006; 65(1):18-25.
5. Hademenos G, Masssoud T, Turjman F, et al. Anatomical and morphological factors correlating with rupture of intracranial aneurysms in patients referred for endovascular treatment. Neuroradiology 1988; 40(11): 755–760.
6. Lall RR, Eddleman CS, Bendok BR, et al. Unruptured intracranial aneurysms and the assessment of rupture risk based on anatomical and morphological factors: sifting through the sands of data. Neurosurg Focus 2009; 26(5):E2.
7. Tremmel M, Dhar S, Levy EI, Mocco J, et al. Influence of intracranial aneurysm-to-parent vessel size ratio on hemodynamics and implication for rupture: results from a virtual experimental study. Neurosurgery 2009; 64(4):622-630.
8. Jeong YG, Jung YT, Kim MS, et al. Size and location of ruptured intracranial aneurysms. J Korean Neurosurg Soc 2009; 45(1):11-5.
9. Jou LD, Mawad ME. Growth rate and rupture rate of unruptured intracranial aneurysms: a population approach. Biomed Eng Online 2009; 8:11.
10. Millán R, Dempere-Marco L, Pozo J, et al. Morphological characterization of intracranial aneurysms using 3D moment invariants. IEEE Trans. Med. Imag 2007; 26(9):1270–1282.
11. De Rooij, Velthuis BK, Algra A, et al. Configuration of the Circle of Willis, Direction of flow, and shape of the aneurysm as risk factors for rupture of intracranial aneurysms. J Neurol 2009; 256(1):45-50.
12. Raghavan ML, Ma B, Harbaugh RE. Quantified aneurysm shape and rupture risk. J Neurosurg 2005; 102(2):355-362.
13. Ma B, Harbaugh RE, Raghavan ML. Three-dimensional geometrical characterization of cerebral aneurysms. Annals of Biomedical Engineering 2004: 32(2):264-273.
14. Hoh BL, Cheung AC, Rabinov JD, et al. Results of a prospective protocol of computed tomographic angiography in place of catheter angiography as the only diagnostic and pretreatment planning study for cerebral aneurysms by a combined neurovascular team. Neurosurgery 2004; 54(6):1329-40.
15. Li Q, Lv F, Li Y, et al. Subtraction CT angiography for evaluation of intracranial aneurysms: comparison with conventional CT angiography. Eur Radiol 2009; 19(9): 2261-2267.
16. Sluzewski M, van Rooij WJ, Slob MJ, et al. Relation between aneurysm volume, packing and compaction in 145 cerebral aneurysms treated with coils. Radiology 2004; 231(3):653-658.
17. Slob MJ, van Rooij WJ, Sluzewski M. Coil thickness and packing of cerebral aneurysms: a comparative study of two types of coils. AJNR Am J Neuroradiol 2005; 26(4): 901-903.
18. Law MWK, Chung ACS. Vessel and intracranial aneurysm segmentation using multi-range filters and local variances. MICCAI 2007; 10(Pt 1):866-874.

19. Hernandez M, Frangi AF. Non-parametric geodesic active regions: method and evaluation for cerebral aneurysms segmentation in 3DRA and CTA. Medical Image Analysis 2007; 11(3):224-241.

20. Caselles V, Kimmel R, Sapiro G. Geodesic active contours. International Journal of Computer Vision 1997; 22(1):61-79.

21. Weickert J. Anisotropic diffusion in image processing. PhD thesis. Department of Mathematics. University of Kaiserslautern. Germany; 1996.

22. Weickert J. Applications of nonlinear diffusion in image processing and computer vision. Acta Math. Univ. Comenianae. 2001; LXX (1):33-50.

23. Prona P, Malik J. Scale space and edge detection using anisotropic diffusion. IEEE Trans. Pattern Anal. Mach. Intell. 1990; 12 (7):629-639.

24. Sethian JA. Level set methods and fast marching methods. ISBN 0521645573. Cambridge University Press; 1999.

25. Sethian JA. A fast marching level set method for monotonically advancing fronts. Proceedings of the National Academy of Sciences 1996; 93(4):1591-1595.

26. Manniesing R, Velthuis BK, van Leeuwen MS, et al. Level set based cerebral vasculature segmentation and diameter quantification in CT Angiography. Medical Image Analysis 2006; 10(2):200-214.

27. Niessen WJ, ter Haar Romeny BM, Florack LMJ, et al. A general framework for geometry-driven evolution equations. International Journal of Computer Vision 1997; 21(3):187-205.

28. Insight Toolkit. Version 3.4. http://www.itk.org.

29. MeVisLab. Version 1.6. Bremen, Germany: MeVis. Medical Solutions AG; 2008.

30. Meijering E, Niessen WJ, Weickert J, et al. Diffusion-enhanced visualization and quantification of vascular anomalies in three-dimensional rotational angiography: results of an in-vitro evaluation. Medical Image Analysis 2002; 6(3):217-235.

31. Ford MD, Hoi Y, Piccinelli M, et al. An objective approach to digital removal of saccular aneurysms: technique and applications. Br J Radiol 2009; 82 Spec No 1: S55-61.

Chapter 3

Quantification of Intracranial Aneurysm Morphodynamics from ECG-gated CT Angiography

ABSTRACT

Rationale and Objectives: Aneurysm morphodynamics is potentially relevant for assessing aneurysm rupture risk. A method is proposed for automated quantification and visualization of intracranial aneurysm morphodynamics from ECG-gated computed tomography angiography (CTA) data.

Materials and Methods: A prospective study was performed in 19 aneurysms from 14 patients with diagnostic workup for recently discovered aneurysms (n=15) or follow-up of untreated known aneurysms (n=4). The study was approved by the IRB (Institutional Review Board) of the hospital and written informed consent was obtained from each patient. An image post-processing method was developed for quantifying aneurysm volume changes and visualizing local displacement of the aneurysmal wall over a heart cycle using multiphase ECG-gated (4D) CTA. Percentage volume changes over the heart cycle were determined for aneurysms, surrounding arteries and the skull.

Results: Pulsation of the aneurysm and its surrounding vasculature during the heart cycle could be assessed from ECG-gated CTA data. The percentage aneurysmal volume change ranged from 3 -18%.

Conclusion: ECG-gated CTA can be used to study morphodynamics of intracranial aneurysms. The proposed image analysis method is capable of quantifying the volume changes and visualizing local displacement of the vascular structures over the cardiac cycle.

This chapter is based on:

Firouzian A, Manniesing R, Metz CT, Risselada R, Klein S, van Kooten F, Sturkenboom MCJM, van der Lugt A, Niessen WJ. Quantification of intracranial aneurysm morphodynamics from ECG-gated CT angiography, Acad Radiol 2012; in press.

INTRODUCTION

Subarachnoid hemorrhage (SAH) caused by rupture of an intracranial aneurysm is a devastating event associated with a high mortality and morbidity rate [1,2]. Risk factors such as smoking, hypertension and alcohol consumption, and aneurysm characteristics including size, location and shape, are known to be important indicators of aneurysm rupture risk [3,4,5,6]. Associations have been found between these risk factors and the static state of the aneurysm. Aneurysmal wall motion may also be considered a risk factor [7] and may provide additional predictive information on rupture risk, as it is related to the mechanical properties of the aneurysmal wall. Several modalities have been used to study aneurysmal wall motion, such as cine phase-contrast magnetic resonance angiography (MRA) [8], transcranial Doppler ultrasound [9], time-resolved rotational angiography [10] and ECG-gated computed tomography angiography (CTA) [11,12,13,14,15]. Of these, ECG-gated CTA is a suitable technique to evaluate aneurysm morphodynamics as it provides high spatial and temporal resolution within a short scanning time. In addition, CTA is used as a routine modality for diagnosis of vascular diseases [11]. Most of these studies focused on aneurysm visualization, apart from a few studies in which aneurysm morphodynamics was quantified manually [16,17]. However, the small size of intracranial aneurysms, their limited volume change over the cardiac cycle, and the limited signal-to-noise ratio (SNR) in 4D CTA, make manual assessment of aneurysmal dynamic behavior a challenging task. Therefore, this study presents an automated image processing method to assess intracranial aneurysm morphodynamics from ECG-gated CTA data to facilitate visualization and quantification of aneurysmal wall motion.

MATERIALS AND METHODS

Patients

Patients aged ≥ 18 years were recruited via the outpatient clinic of the Department of Neurology. With the approval of the Institutional Review Board (IRB), an additional ECG-gated CTA of the intracranial circulation was performed for the purpose of this study and all patients gave written informed consent. In total 14 patients (5 men and 9 women, age range 47-70 years) with 19 unruptured aneurysms were included, who were scanned as a diagnostic workup for a recently discovered unruptured aneurysm or follow-up of a known untreated aneurysm in the period February 2008 to November 2009.

Scan Protocol

Patients were consecutively recruited and scanned with a dual-source 32-detector multidetector CT scanner (Siemens, Somatom Definition, Erlangen, Germany), with collimation of 64x0.6 mm with z-flying focal spot and a maximally obtainable temporal resolution of 83 ms.

First, a routine clinical non-gated CTA of the Circle of Willis was performed, covering 10 cm. In this scan a contrast-enhanced protocol was used: 120 kVp, 150 effective mAs, and pitch 0.7. All patients received 80 ml of contrast material (Iodixonal 320 mgI/ml, Visipaque, GE Healthcare) via the antecubital vein followed by 45 ml saline bolus chaser, each at an injection rate of 4 ml/s. Subsequently, the CTA scan was analyzed by an expert radiologist (AvdL, ≥ 5 years of experience) to detect the target aneurysms and record their maximum size. Second, for the purpose of the study, an ECG-gated CTA was performed with a scan range of 5 cm centered at the aneurysm(s) and all patients received an additional 60 ml of contrast material followed by 40 ml of saline bolus chaser (4 ml/s). The parameters were 120 kVp and 160 mAs / rotation and the pitch was variable by heart rate (0.2-0.43). For both scans, synchronization between the passage of contrast material and data acquisition was achieved by real-time bolus tracking at the level of the common carotid artery (CCA). No medication was used to reduce the heart rate during scanning. The ECG-gated CTA was used to reconstruct multiphase 3D datasets at 5% steps of the cardiac R-R interval, resulting in 20 time-resolved 3D CTA datasets. Image reconstructions were made with a 12.0 cm field of view, a matrix size of 512x512, a slice thickness of 0.75 mm, a reconstruction increment of 0.4 mm, and an intermediate sharp (B31F) reconstruction kernel. The scanning time for the ECG-gated CTA scan ranged from 2.0-4.3 s. Radiation dose from the clinical scan was estimated with CRP103 head dose-length product (DLP) conversion factor of 0.0021 at 0.6 mSv and the additional scan at 0.3-0.8 mSv, depending on the heart rate.

Image Processing Method

The image post-processing method consists of two steps: registration of the multiphase 3D (4D) data to acquire the deformation field which describes the local deformation of image structures in all phases, and aneurysm segmentation. Combining the aneurysm segmentation and estimated deformations, the aneurysmal wall deformation is determined. Each step is explained in detail below.

Registration Method

Nonrigid B-spline registration of the multiphase 3D data is used to estimate the deformation which is present in the dynamic time series. It is directly applied to the dynamic time series, imposing the constraint that the motion should be smooth over time (i.e. continuous and differentiable at all phases) [18,19]. The resolution of the 4D B-spline control point grid that models the deformation was set to 8 mm in the spatial dimension and every other phase (10% of the heart cycle) in the time dimension. These settings allow capturing small motions while still being robust against noise. The method aligns all phases simultaneously without being biased towards one of the phases by minimizing the intensity variance at corresponding voxel locations over time. This results in 1) a motion compensated multiphase 3D image (i.e. it is corrected for deformation between phases), and 2) a deformation field for each phase represented by a vector image (which indicates how much each voxel has moved with respect to the average of all phases).

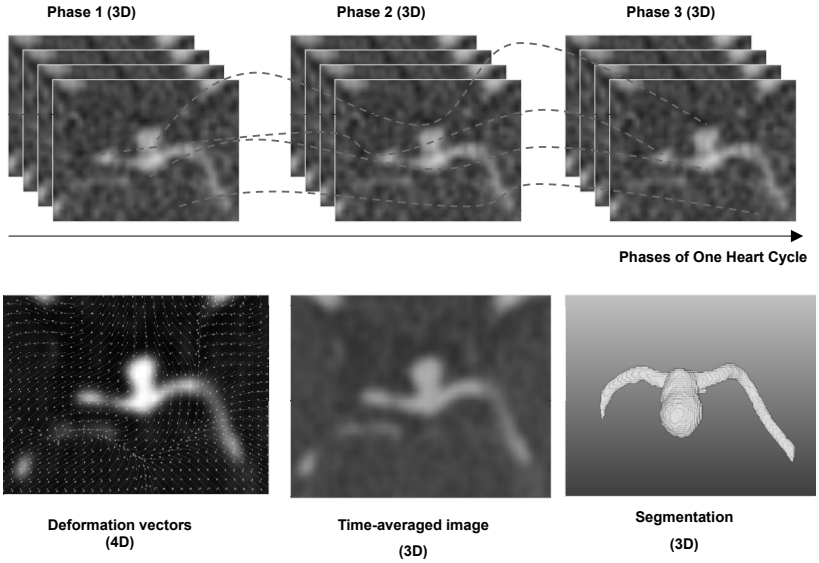

Figure 1. Top row: a schematic drawing of the 4D registration method. Dashed lines show how voxels are displaced to be aligned with the corresponding voxels in other phases. Bottom row: an example of the deformation vector field, time-averaged image and segmentation from the same dataset.

A 3D image with improved SNR is created by averaging all motion compensated images over time (Figure 1). This image is denoted the time-averaged 3D image and is used for aneurysm segmentation.

Segmentation Method

To study the dynamic behavior of the anatomical structures of interest, the aneurysm and surrounding arteries were segmented. The segmentation method is a 3D semi-automatic method based on a geodesic active contours (GAC) framework [20,21] and is performed on the time-averaged 3D image. The method is initialized by a small spherical surface, centered at a user-defined seed point within the aneurysm. This surface then evolves with a speed depending on three different image features, i.e. image intensity, image gradient, and image intensity variation. These features are calculated around the user-defined seed point inside the aneurysm. Details on the speed function, which was previously optimized for segmentation accuracy, can be found in [22]. The result of this segmentation includes the aneurysm and surrounding arteries. For validation purposes, part of the skull was also segmented using a seeded region growing method [23] initialized by user-selected seed points and using image intensity information within the HU range of 400-1530.

Volume Quantification

For each phase *i*, relative volume change (k_i) of an anatomical structure (aneurysm, artery, bone) can be derived from the deformation field provided by the registration method. k_i represents the amount of expansion or shrinkage at each voxel in each phase with respect to the average volume of the structure over the heart cycle (v_{avg}). This average volume can be determined by calculating the volume of the segmented structure in the time-averaged 3D image [24]. The absolute volume at each phase (v_i) is obtained by the equation $\left(v_i = k_i \times v_{avg} \right)$. This holds for all of the anatomical structures.

Experimental details

To analyze morphodynamics of the aneurysm and surrounding arteries, the method was applied to a region of interest (ROI) of 3x3x3 cm around the aneurysm. This region was created by cropping the image at a distance of 3 cm in each spatial direction from a user-defined point inside the aneurysm. To study aneurysms and vessels separately, following segmentation the aneurysm was manually separated from the surrounding arteries by an expert radiologist (AvdL) using a dedicated software tool [25]. The separation was performed by drawing 2D contours around the aneurysm slice by slice to define the aneurysm neck location. To compare dynamic behavior of aneurysms and healthy surrounding vasculature, we compared diameter changes over the heart cycle. To obtain a single value which represents the equivalent diameter of each structure, we assumed 'aneurysm' as if it would be a spherical object[1] and 'vessel' as if it would be a cylindrical object[2].

The volume changes during the heart cycle were presented in graphs. Additionally, for validation purposes, the volume change of a piece of skull as a function of cardiac phase was assessed.

In the absence of a ground truth for aneurysm morphodynamics, we performed an additional evaluation using simulated data. Hereto, simulated 4D CTA series were created by applying each of the 19 (4D) deformation fields found by the registration method in the first experiment to their next baseline 3D CTA scan and creating 19 new time series. Using this design, the ground truth deformations are known.

We chose to use simulated data, as it produces image series with realistic dynamic behavior and image appearance, which would be very difficult to obtain using a physical phantom. The aneurysm deformation recovered by the algorithm was compared to the known deformation and the difference was calculated as an error measure.

Acquiring and using the ECG-gated CTA data for this study was approved by the IRB of the hospital in May 2007.

---

1 $v = \frac{4}{3}\pi r^3$

2 $v = \pi r^2 l$;The lengths of the arteries (l) were also measured to allow calculation of vessel diameter from a known volume

RESULTS

The patients included in the present study had a mean heart rate of 77±17 bpm and the maximum diameter of the aneurysms ranged from 2-19 (7.6 ± 3.8) mm; these data were extracted from the patient reports. Table 1 presents a summary of the quantitative analysis on 19 aneurysms and surrounding vessels from 14 patients. The percentage volume change ($\%v_{change} = \frac{v_{\max} - v_{\min}}{v_{\min}} \times 100$) of the aneurysms was calculated based on the difference between maximum $v_{\max}$ ($v_{\max} = k_{\max} \times v_{avg}$) and minimum volume $v_{\min}$ ($v_{\min} = k_{\min} \times v_{avg}$) over the heart cycle and was equal to 8.0% ± 4.6% (range 3-18%). In contrast, and as expected, in bone tissue there was no substantial change in percentage volume change (1.9% ± 1.7%; range 0.4-5.6%).

Both in the aneurysm and surrounding vasculature, the relative volume change versus time graphs had multiple peaks (Figure 2) and for each aneurysm not necessarily in the same phase as the corresponding surrounding vasculature. The relative volume change of aneurysms versus their minimum volume $v_{\min}$ including their location on the Circle of Willis is shown in Figure 3. A low correlation between aneurysm size and its volume change in a heart cycle was observed (correlation coefficient = 0.4).

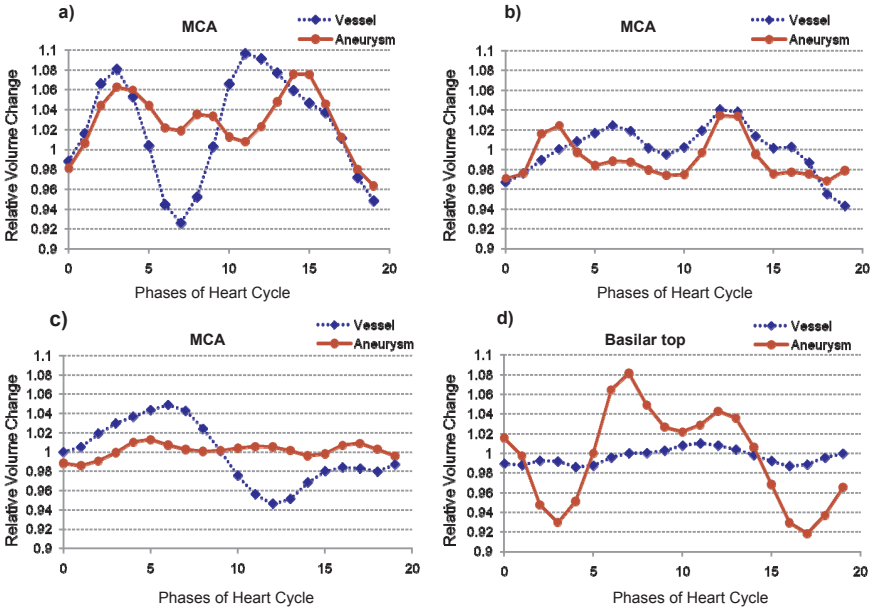

Figure 2. Aneurysm volume as function of cardiac cycle obtained with the automated image processing method. Each graph shows the relative volume change with respect to the average volume for aneurysm and its surrounding vessel as a function of cardiac phase. The aneurysms in the top row have the same location but difference sizes: a) Middle cerebral artery (10 mm), b) Middle cerebral artery (8 mm), and the bottom pair have the same size but different locations: c) Basilar tip (8 mm) and d) Middle cerebral artery (8 mm).

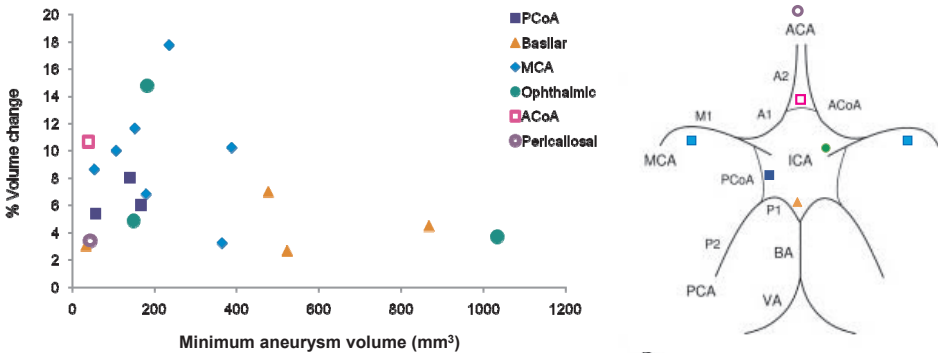

Figure 3. Percentage volume change in 19 aneurysms as a function of their minimum volume in the cardiac cycle (left). The aneurysms with the same location are represented with the same symbol. On the right, there is a schematic drawing of the Circle of Willis indicating the aneurysm locations.

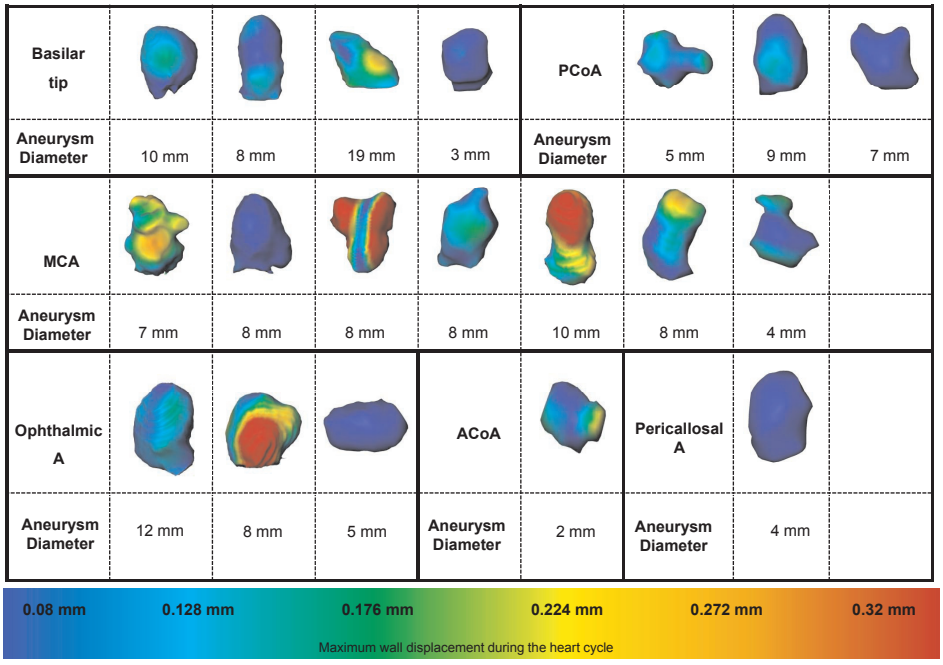

Figure 4. Maximum local displacement of the aneurysmal wall in mm with respect to the phase of the heart cycle with minimum volume, presented by colors on the 3D volume rendered segmentation of the aneurysm domes. The domes are arranged in rows (from left to right the diameter decreases) and the locations are mentioned next to each row. All the aneurysms are oriented such that their neck is downwards and their head upwards. The color scale is shown in the bottom part of the figure (0.08-0.32 mm). The values below 0.08 are shown in dark blue and above 0.32 in red in order to increase the color resolution of the figure.

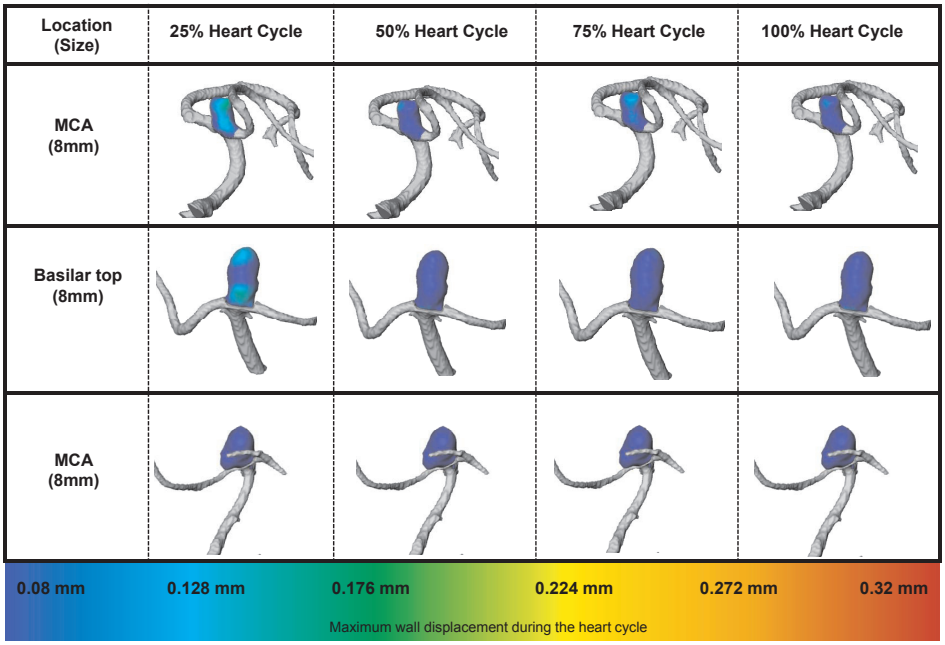

Figure 5. Four time frames (25%, 50%, 75% and 100% of the heart cycle) of three aneurysms with similar size (≈ 8 mm) but different locations are presented. The color code represents maximum local displacement of the dome with respect to the phase with minimal aneurysm volume.

Regarding the location, basilar tip aneurysms showed less volume change compared to the others. Diameter change of aneurysms was significantly larger than of vessels (0.17 ± 0.1 versus 0.1 ± 0.06 mm, p-value = 0.018).

A color-coded presentation of the maximum local wall displacement of all investigated aneurysms is shown in Figure 4. In this figure, global translations of the entire aneurysms were subtracted before calculating the displacements. This figure suggests that aneurysm shape may influence the dynamic behavior, in addition to size and location. Figure 5 illustrates the dynamic behavior of four aneurysms by visualizing the local wall displacement in 4 of 20 phases, including the phases at 25%, 50%, 75% and 100% of the heart cycle, using color coding. With this visualization, it is possible to follow wall displacement at every point over time.

Results on the simulated 4D CTA data show that the residual volume change due to imperfect registration was 4.2 ± 2.1%, which is significantly smaller than the deformations found in the original data (p-value=0.006).

Statistical analysis

Statistical analysis was performed using the software package SPSS (Illinois, USA), Version 15.0 for Windows. The data groups were compared using the Wilcoxon Signed-Ranks Test and p-values ≤ 0.05 were considered statistically significant.

Table 1. Summary of the patient information and aneurysm morphology and morphodynamics in 19 aneurysms and their neighboring arteries from 14 patients are presented in this table.

Patient			Aneurysm						Artery	
No.	Sex	Age	No.	Location*	Size (mm)	V_{min} (mm^3)	$\%V_{change}$	d_{max}-d_{min} (mm)	$\%V_{change}$	d_{max}-d_{min} (mm)
1	F	50	1	Basilar tip	3	33	3.1	0.040	3.5	0.044
2	M	70	2	PCoA L	9	139	8.0	0.168	15.1	0.162
2	M	70	3	PCoA R	7	56	5.4	0.084	13.1	0.175
3	F	55	4	PCoA R	5	166	6.0	0.135	14.3	0.200
3	F	55	5	ACoA L	2	38	10.7	0.143	6.2	0.082
4	F	60	6	Ophthalmic A L	5	149	4.9	0.105	2.0	0.024
5	F	63	7	MCA R	8	179	6.8	0.155	10.3	0.010
5	F	53	8	MCA L	4	53	8.6	0.131	6.9	0.090
6	M	47	9	Basilar tip	19	476	7.0	0.221	8.5	0.100
7	F	67	10	MCA L	8	235	17.7	0.428	2.4	0.026
8	M	68	11	Basilar tip	10	867	4.5	0.175	5.5	0.094
8	M	68	12	MCA L	7	387	10.2	0.300	5.4	0.053
9	F	52	13	MCA R	10	151	11.6	0.247	18.4	0.175
10	F	57	14	Ophthalmic A L	8	182	14.8	0.331	8.1	0.100
11	M	61	15	MCA L	8	106	10.0	0.190	8.5	0.118
12	F	57	16	Ophthalmic A L	12	1033	3.7	0.154	3.5	0.042
13	M	70	17	Basilar tip	8	522	2.7	0.100	10.9	0.200
14	F	54	18	MCA L	8	363	3.2	0.100	2.7	0.033
14	F	54	19	Pericallosal A	4	42	3.4	0.050	2.6	0.025

* ACoA, Anterior Communicating Artery; L, Left; MCA, Middle Cerebral Artery; PCoA, Posterior Communicating Artery; R, Right.

DISCUSSION

To our knowledge, an automated method for quantification of intracranial aneurysm morphodynamics from ECG-gated CTA has not been presented previously. Results of applying our method to19 unruptured aneurysms suggest that the amount of volume change as estimated by the method is not directly related to aneurysm size and thus may provide additional information in predicting rupture risk. Potentially, there could be a relation between aneurysm volume change and location; however, due to the limited amount of data in the present study we were unable to investigate this aspect.

Since the aneurysm wall has different properties than a healthy vessel segment, it is expected that aneurysms have larger volume changes over the cardiac cycle which was indeed observed in this study. No significant volume change in the bone area, suggests that the reported

changes are due to actual aneurysmal wall motion and are not due to image reconstruction errors, noise, or other artifacts.

The observed deformation of aneurysms in our study was small. By utilizing B-splines to model aneurysm deformation it is possible to estimate subvoxel motion and obtain measurements at every point along the spline.

Recent studies [16,17] on intracranial vasculature dynamics have used thresholding and manual interactions for visualizing and quantifying vascular deformation. Considering the low resolution, noise, and small size of aneurysms, accurate segmentation and volume measurements in dynamic data is challenging when relying only on intensity values in each phase. The possible variations of intensity in different phases of the time series, artifacts and patient motion should be taken into account. The method proposed in this chapter utilizes information over the whole time series, and is automated. Regarding the results, it has been shown in [16,17] that aneurysm volume change over the cardiac cycle (in most cases) has two peaks resembling an arterial pulse wave [26]. Although the results of the present study are in agreement with this, in 50% of the cases the aneurysm volume changes happen to have a small third peak. This is probably due to the fact that arterial wall motion is the result of pressure difference between the inside and outside of the artery; for aneurysms, since the outside pressure (intracranial pressure) is variable [9,27], a behavior different from that in CCA can be expected. Furthermore, the reflection waves along the arterial tree [28], the unstable structure of aneurysms, and the complicated geometry of the Circle of Willis (from a hemodynamic point of view), should also be taken into account.

To conclude, the proposed automated image processing method is capable of quantifying intracranial aneurysm volume changes and visualizing local aneurysmal wall motion from ECG-gated CTA during a heart cycle. This analysis provides additional information on the status of the aneurysmal wall which, together with other geometrical information, may help to better estimate aneurysm growth and predict rupture risk. Further research in a prospective setting is required to determine the additional value of aneurysm morphodynamics in the context of aneurysm growth and rupture risk prediction.

REFERENCES

1. Huang J, van Gelder JM. The probability of sudden death from rupture of intracranial aneurysms: A meta-analysis. *Neurosurgery* 2002; 51:1101-1105.
2. Brisman JL, Song JK, Newell DW. Medical Progress: Cerebral Aneurysms. N Engl J Med 2006; 355:928-939.
3. Schievink WI. Intracranial Aneurysms. N Engl J Med 1997; 336:28-40.
4. Hademenos GJ, Masssoud TF, Turjman F, et al. Anatomical and morphological factors correlating with rupture of intracranial aneurysms in patients referred for endovascular treatment. Neuroradiology 1988; 40:755-760.
5. Lall RR, Eddleman CS, Bendok BR, et al. Unruptured intracranial aneurysms and the assessment of rupture risk based on anatomical and morphological factors: sifting through the sands of data. Neurosurg Focus 2009; 26:E2.
6. Jeong YG, Jung YT, Kim MS, et al. Size and location of ruptured intracranial aneurysms. J Korean Neurosurg Soc 2009; 45:11-15.
7. Hayakawa M, Maeda S, Sadato A, et al. Detection of pulsation in ruptured and unruptured cerebral aneurysms by electrocardiographically gated 3-dimensional computed tomography with a 320-row area detector computed tomography and evaluation of its clinical usefulness. Neurosurgery 2011, 69(4):843-851.
8. Meyer FB, Huston J 3rd, Riederer SS. Pulsatile increases in aneurysm size determined by cine phase-contrast MR angiography. J Neurosurg 1993; 78: 879-883.
9. Wardlaw JM, Cannon, Statham PF, et al. Does the size of intracranial aneurysms change with intracranial pressure? Observations based on color "power" transcranial Doppler ultrasound. J Neurosurg 1998; 88:846-850.
10. Zhang C, Villa-Uriol MC, De Craene M, et al. Morphodynamic analysis of cerebral aneurysm pulsation from time-resolved rotational angiography. IEEE Trans Med Imaging 2009; 28:1105-1116.
11. Ishida F, Ogawa H, Simizu T, et al. Visualizing the dynamics of cerebral aneurysms with four-dimensional computed tomographic angiography. Neurosurgery 2005; 57:460-471.
12. Hayakawa M, Katada K, Anno H, et al. CT angiography with electrocardiographically gated reconstruction for visualizing pulsation of intracranial aneurysms: Identification of aneurysmal protuberance presumably associated with wall thinning. Am J Neuroradiol 2005; 26:1366-1369.
13. Kato Y, Hayakawa M, Sano H, et al. Prediction of impending rupture in aneurysms using 4D-CTA: Histopathological verification of a real-time minimally invasive tool in unruptured aneurysms. Minim Invasive Neurosurg 2004; 47:131-135.
14. Yaghmai V, Rohany M, Shaibani A, et al. Pulsatility imaging of saccular aneurysm model by 64-slice CT with dynamic multiscan technique. J Vasc Interv Radiol 2007; 18:785-788.
15. Umeda Y, Ishida F, Hamada K, et al. Novel dynamic four-dimensional CT angiography revealing 2-type motions of cerebral arteries. Stroke 2011; 42:815-818.
16. Nishada T, Kinoshita M, Tanaka H, et al. Quantification of cerebral artery motion during the cardiac cycle. AJNR 2011; 32:E206-208.

17. Kuroda J, Kinoshita M, Tanaka H, et al. Cardiac cycle-related volume change in unruptured cerebral aneurysms: a detailed volume quantification study using 4-dimensional CT angiography. Stroke 2012, 43:61-66.

18. Metz CT, Klein S, Schaap M, et al. Nonrigid registration of dynamic medical imaging data using nD+t B-splines and a groupwise optimization approach. Med Image Anal 2011; 15:238-249.

19. Klein S, Staring M, Murphy K, et al. elastix: a toolbox for intensity-based medical image registration. IEEE Trans Med Imaging 2010; 29:196-205.

20. Caselles V, Kimmel R, Sapiro G. Geodesic active contours. Int J Comp Vision 1997; 22:61-79.

21. Sethian JA, Level set methods and fast marching methods. Cambridge University Press; 1999: 1-13.

22. Firouzian A, Manniesing R, Flach HZ, et al. Intracranial aneurysm segmentation in 3D CT angiography: Method and quantitative validation with and without prior noise filtering. Eur J Radiol 2010 ; 79:299-304.

23. Adams R, Bischof L. Seeded region growing. IEEE Trans Pattern Anal Machine Intell 1994; 16:641-647.

24. Riddle WR, Li R, Fitzpatrick JM, et al. Characterizing changes in MR images with color-coded Jacobians. Magn Reson Imaging 2004; 22:769-777.

25. MeVisLab. Version 1.6. Bremen, Germany: MeVis Medical Solutions AG; 2008.

26. Laurent S, Cockcroft J, Van Bortel L, et al. Expert consensus document on arterial stiffness: methodological issues and clinical applications. Eur Heart J 2006; 27: 2588-2605.

27. Alperin N, Mazda M, Lichtor T, et al. From cerebrospinal fluid pulsation to noninvasive intracranial compliance and pressure measured by MRI flow studies. Curr Med Imaging Rev 2006; 2:117-129.

28. Nichols WW, O'Rourke M F. McDonald's Blood Flow in Arteries: theoretical, experimental and clinical principles. 3rd ed. London: Edward Arnold; 1990.

Chapter 4

Intracranial aneurysm growth quantification in CTA

ABSTRACT

Next to aneurysm size, aneurysm growth over time is an important indicator for aneurysm rupture risk. Manual assessment of aneurysm growth is a cumbersome procedure, prone to inter-observer and intra-observer variability. In clinical practice, mainly qualitative assessment and/or diameter measurement are routinely performed. In this chapter a semi-automated method for quantifying aneurysm volume growth over time in CTA data is presented. The method treats a series of longitudinal images as a 4D dataset. Using a 4D groupwise non-rigid registration method, deformations with respect to the baseline scan are determined. Combined with 3D aneurysm segmentation in the baseline scan, volume change is assessed using the deformation field at the aneurysm wall. For ten patients, the results of the method are compared with reports from expert clinicians, showing that the quantitative results of the method are in line with the assessment in the radiology reports. The method is also compared to an alternative method in which the volume is segmented in each 3D scan individually, showing that the 4D groupwise registration method agrees better with manual assessment.

This chapter is based on:

Firouzian A, Manniesing R, Metz CT, Klein S, Velthuis BK, Rinkel GJE, van der Lugt A, Niessen WJ. Intracranial aneurysm growth quantification in CTA, SPIE Medical Imaging 2012; Proc. of SPIE 8314, 831448.

INTRODUCTION

Aneurysmal subarachnoid hemorrhage (aSAH) has a high mortality rate and approximately half of the survivors experience irreversible brain damage [1]. People with familial intracranial aneurysm or a history of aSAH are at high risk of aneurysm formation and rupture and should be screened [2,3]. Aneurysm growth over time is an important predictor of aneurysm rupture since enlarging aneurysms are unstable and more prone to rupture. Some follow-up studies have been performed to model aneurysm growth and rupture rate [4-9]. In other studies patients with aneurysms after aSAH had follow-up imaging with Magnetic Resonance Angiography (MRA) [10-12] or Computed Tomography Angiography (CTA) [3,13] which lead to valuable information on aneurysm growth, formation of new aneurysms and treatment planning.

As aneurysm growth is typically small over the time window of interest, it is very difficult to accurately measure it. Size and location have been studied as potential predictors of aneurysm growth. Studies using MRA showed that location is not an important predictor for growth [10,11]. In contrast, size is a very good predictor for growth and aneurysms with a diameter larger than 8-9 mm have the highest probability of growth and rupture [10-12] but this does not imply that small aneurysms do not grow [5,10].

Performing accurate measurements of changes in aneurysm size could provide valuable information to investigate the determinants of growth, predict rupture risk and guide clinical decision-making. So far, all studies have relied on manual measurements of aneurysm size and growth. These measurements are prone to inter- and intra-observer variability. Therefore, there is a need for an automated method, which can perform the measurements more accurately, consistently and objectively.

METHOD

In this chapter two post-processing methods for intracranial aneurysm growth quantification in CTA data acquired in a longitudinal study are considered (Figure 1). The first method (Figure 1a)) is a new approach, which treats a longitudinal series of images as a time series (4D) image, and utilizes 4D groupwise registration, in combination with aneurysm segmentation of the first time point (TP) scan to determine aneurysm growth. The second method (Figure 1 b)) is based on the application of a 3D segmentation method, previously presented in [14], to each time point individually.

In both methods 3D CTA images from series of longitudinal images of each patient are aligned with the first TP using rigid registration to compensate for any displacement or rotation of the head during scanning. Subsequently, a 3x3x3 cm Region of Interest (ROI) around the aneurysm is selected by a user defined point inside the aneurysm in the first TP. Using the results of rigid registration, the chosen point is mapped to all other TPs in the time series; so that

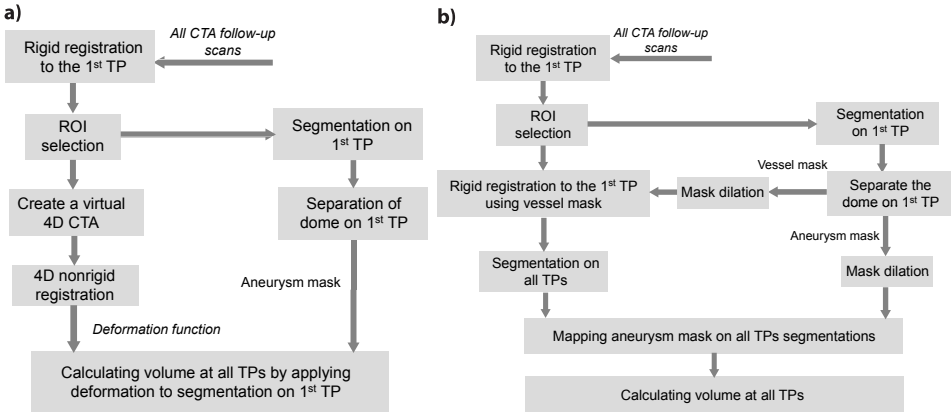

Figure 1. Block diagram of the two quantification methods for intracranial aneurysm growth used in this study: a) treating a longitudinal series of images as a 4D image and b) treating each image in the series individually.

all ROIs correspond. Segmentation is then performed on the baseline scan using the Geodesic Active Contours (GAC) frame work. The segmentation is represented by the zero level set of an embedding function Φ which is initialized with a spherical surface centered at a user defined seed point inside the aneurysm area [15,16]. The evolution of Φ is governed by:

$$\Phi_t - \mu \nabla F \nabla \Phi + F(1 - \varepsilon k_{mean}) \left| \nabla \Phi \right| = 0 \tag{1}$$

where *F* is a speed function, ε is a weighting factor which determines the influence of the surface smoothness term, k_{mean} is the mean curvature, and μ is the weighting factor of the advection term. The speed function (*F*) should be selected such that the evolution of the surface halts at the aneurysm boundary. In our method, it is defined using three image features, namely: intensity (F_i), intensity variation (F_n) and intensity gradient (F_{grad}):

$$F = F_i . F_{grad} . F_n \tag{2}$$

The intensity based speed function is defined as follows:

$$F_i(\vec{x}) = \frac{g_v(\vec{x}) - g_b}{g_v(\vec{x}) + g_b} \tag{3}$$

Where $g_v(\vec{x})$ and g_b are estimates of the aneurysm and background intensity distribution respectively.

The second feature is the gradient magnitude:

$$F_{grad}(\vec{x}) = e^{-\left(\frac{|\nabla I(\vec{x})|}{\gamma}\right)^2} \quad (4)$$

where $|\nabla I(\vec{x})|$ is the gradient magnitude of the image I and γ is a tuning factor.
The third feature is intensity variance which is formulated as follows:

$$F_n(\vec{x}) = e^{-\left(\frac{\sigma(\vec{x})}{\beta}\right)^2} \quad (5)$$

where σ is the local standard deviation of the intensity values and β is a tuning factor.

Upon convergence, the aneurysm and surrounding vasculature are extracted from the level set, resulting in a binary mask. As we are only interested in the aneurysm volume, we separate the aneurysm from the surrounding vasculature using an automated method which uses three or four user defined seed points depending on the geometry of the aneurysm (Figure 2). The first seed point is placed inside the aneurysm and the other seed points in each vessel branch proximal and distal to the aneurysm. In the next step, the centerlines between each pair of seed points are calculated using the Vascular Modeling Toolkit (vmtk) [17,18]. In this approach a number of spheres are fitted inside the vessel's surface and the center of these spheres determine the centerline. By thresholding the distance transform on the level set image from the segmentation method iteratively at different values, we can check when the point inside the aneurysm is separated from the other points in the vessels. As soon as they are separated, the iteration will stop and the aneurysm mask will be generated. Recently, another approach for aneurysm separation which uses centerlines as well has been published [19].

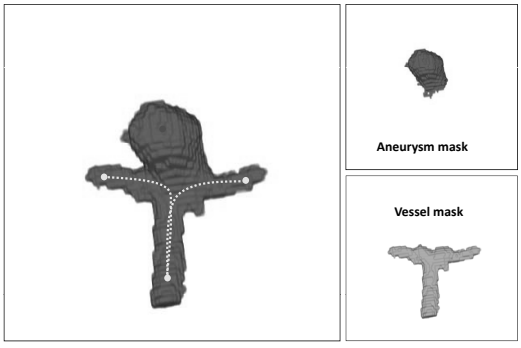

Figure 2. Schematic drawing showing separation of aneurysm from surrounding vasculature of an aneurysm located on the basilar tip. The user defined points and paths found by the algorithm are shown on the segmentation (left). The aneurysm and vessel masks after separation are shown as well (right).

The aforementioned steps are identical for both methods. The methods differ when it comes to calculating the aneurysm volume in different TPs. In the first method (Figure 1 a)) all the ROI images of each series are concatenated and a virtual 4D ROI image is created. A 4D nonrigid registration method is then applied to spatially align all TPs simultaneously in a groupwise manner, thus obtaining the corresponding deformations for each TP [20-23]. The nonrigid registration method consists of a stack of independent 3D free form B-spline transformations and is not biased towards a certain time point. The free form transformation model is described as follows:

$$\vec{T}_{\vec{\mu}}(\vec{y}) = \vec{y} + \sum_{\vec{y}_k \in N_{\vec{y}}} \begin{bmatrix} \vec{p}_k \\ 0 \end{bmatrix} \beta^r(\vec{y} - \vec{y}_k) \tag{6}$$

with $\vec{T}_{\vec{\mu}}$ the transformation of the 4D image, $\vec{y}_k$ the control points, $\beta^r(\vec{y})$ the r-th order three-dimensional B-spline polynomial, $\vec{p}_k$ the 3D B-spline coefficient vectors, $N_{\vec{y}}$ the set of all control points within the compact support of the B-spline at $\vec{y}$, and μ a vector of transformation parameters that consists of all the values of $\vec{p}_k$ concatenated. The additional zero value in the B-spline summation reflects that displacements in the time direction are not allowed. Our objective is to find the deformations that best spatially align the different TPs. Hereto, we minimize the intensity variations over time, and the dissimilarity metric is hence defined as:

$$C(\vec{\mu}) = \frac{1}{|S||\tau|} \sum_{\vec{x} \in S} \sum_{t \in \tau} (I(\vec{T}_{\vec{\mu}}(\vec{x}, t)) - \bar{I}_{\vec{\mu}}(\vec{x}))^2 \tag{7}$$

with $\bar{I}_{\mu}(\vec{x})$ the average intensity value over time at location $\vec{x}$ after applying transformation $\vec{T}_{\vec{\mu}}$:

$$\bar{I}_{\vec{\mu}}(\vec{x}) = \frac{1}{|\tau|} \sum_{t \in \tau} I(\vec{T}_{\vec{\mu}}(\vec{x}, t)) \tag{8}$$

and S and τ are the set of spatial and temporal voxel coordinates respectively.

After optimization, the deformation with respect to the baseline scan is found by composition of the forward and inverse transformation $\vec{T}_{\vec{\mu}}(\vec{T}_{\vec{\mu}}^{-1}(\vec{x}, 0), t)$, as explained in [20]. The relative volume change of the aneurysm is calculated by averaging the Jacobian determinant of the transformation in the aneurysm area (*m*) using the aneurysm mask created from the segmentation. Considering the aneurysm volume in the baseline scan as v_0, the follow up volume *v* is calculated as: $v = m \cdot v_0$.

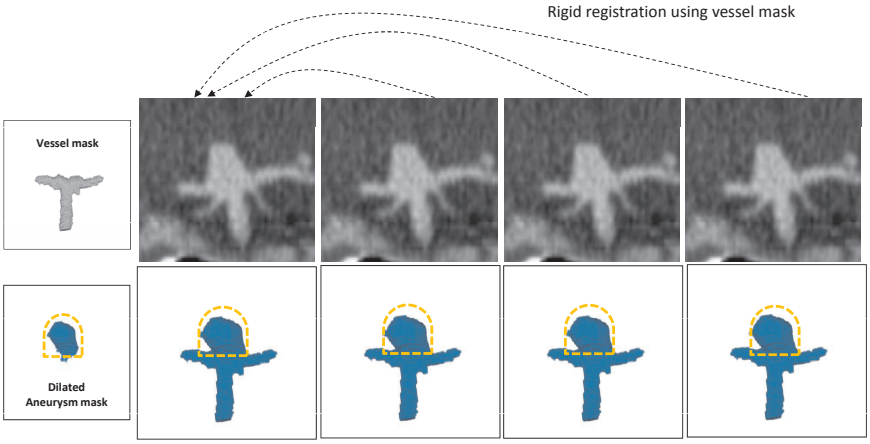

Figure 3. Schematic drawing of the second method to quantify aneurysm growth. First row: longitudinal series of CTA images of a basilar tip aneurysm. Second row: aneurysm segmentation performed at each time point. The vessel and aneurysm masks created from the segmentation on the baseline scan are shown on the right. The dotted line around the aneurysm shows the region in which the aneurysm volume is calculated.

In the second method (Figure 1 b)) each TP scan is analyzed separately. To measure growth, the aneurysm neck should be defined at the same anatomical location in all scans. For this purpose, assuming that the vessels will not deform between the different acquisitions, all the follow-up scans are rigidly aligned using the vessel mask from the baseline scan. Segmentation is then performed in all TP scans using the same method as applied in the baseline scan. Having the aneurysm mask available from the baseline, we dilate it by 4 voxels keeping the neck area unchanged. The dilated mask will define the region in which we will measure aneurysm volume in follow-up scans and calculate the aneurysm volume change (Figure 3).

RESULTS

Both methods were applied to longitudinal CTA series from 10 randomly selected patients. These patients with a history of subarachnoid hemorrhage from a ruptured aneurysm had a follow-up as a clinical routine to monitor other unruptured aneurysms. The age range was between 42 and 73 years at the time of screening and all patients were female. We selected the first and the last scan available for each patient to measure the maximum growth during the follow-up period. For all scans the patient report was available from which we retrieved the radiologist's report on aneurysm growth. Using this information, we compared the performance of both automated methods with the clinical diagnosis.

In clinical practice, aneurysm diameter is the parameter which is most commonly used to report aneurysm growth. Therefore the aneurysm diameter change was calculated from the volumes at baseline and follow-up assuming a spherical shape. The results of the study are

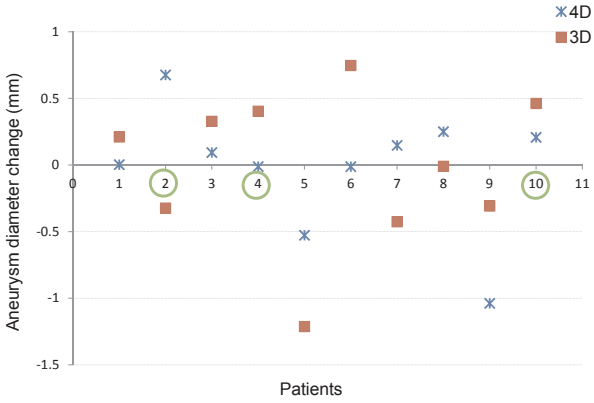

Figure 4. Diameter change of aneurysm calculated using the 4D and 3D methods between baseline and follow-up scan for 10 patients. The green circles on the horizontal axis indicate the patients for whom growth was reported in their clinical reports.

Table 1. Quantitative results of base volume, location and calculated diameter change of all aneurysms using both the 3D and 4D method compared to the qualitative results from the manual assessment.

	Locations*	Base Vol. (mm^3)	Diameter change (mm) 3D	Diameter change (mm) 4D	Growth? (manual)
1	Basilar tip	146.82	0.21	0.003	N
2	PCoA R	59.23	-0.32	0.67	Y
3	ACoA L	10.06	0.33	0.09	N
4	MCA L	19.40	0.40	-0.01	Y
5	Basilar tip	217.53	-1.21	-0.53	N
6	Basilar tip	9.08	0.75	-0.012	N
7	ACoA L	97.89	-0.42	0.15	N
8	MCA R	59.08	-0.01	0.25	N
9	ICA R	81.20	-0.31	-1.04	N
10	MCA R	14.21	0.46	0.21	Y

* ACoA, Anterior Communicating Artery; ICA, Internal Carotid Artery; L, Left; MCA, Middle Cerebral Artery; PCoA, Posterior Communicating Artery; R, Right.

presented in Figure 4. For three out of ten aneurysms, growth was reported in the patient reports which are indicated by a circle in the figure. Both quantification methods were applied to all data sets and the difference in diameter between the baseline and follow-up scan are presented. The 4D method has more agreement with the patient reports than the 3D method. The 3D method did find decrease in diameter (which is unlikely) in four out of ten cases while there was no change reported in the reports and 4D method found two. Case 5 is an exception since it has a thrombus inside which causes the lumen size to decrease. Detailed information

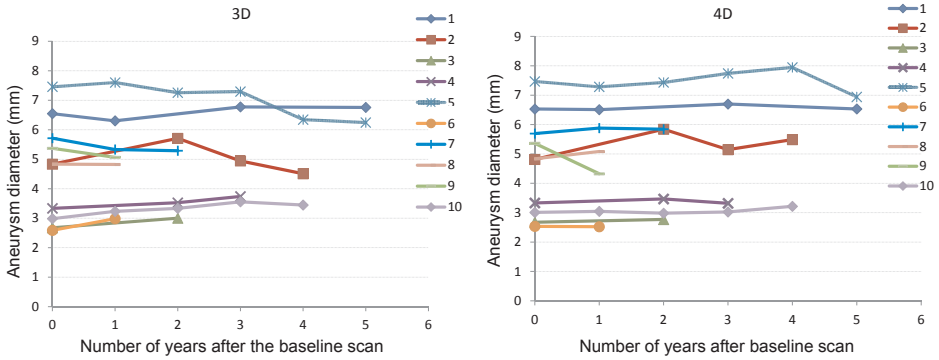

Figure 5. Aneurysm diameter over time for all data sets using the 4D (on the left) and 3D (on the right) methods.

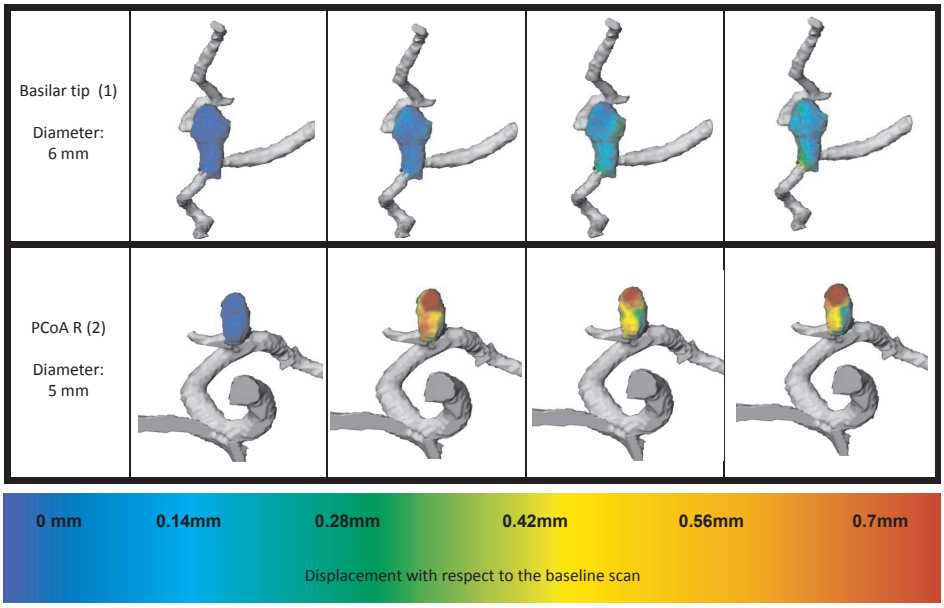

Figure 6. Color coding the amount of displacement with respect to the baseline scan. Each row shows one aneurysm in different time points (from left to right). The top aneurysm is the case No. 1 which is located at the basilar tip and the bottom aneurysm is case No. 2 which is located at PCoA R.

about each aneurysm is presented in Table 1, including location, volume, diameter change using each method and the qualitative manual assessment derived from the patient reports.

Additionally, to elucidate the difference between two methods, for all aneurysms, the diameter at all scan time points was calculated which is shown in Figure 5. The number of TPs for each aneurysm is different depending on the available scans in the period of the study. Overall the 4D method results are smoother over time as compared to the results obtained with the 3D method.

Using the 4D method it is also possible to measure the local displacements which potentially give us the possibility to investigate the parts of the aneurysm that are more prone to rupture. Figure 6 shows two aneurysm segmentations in which the displacement at each voxel is color coded, making it easy to identify the regions which deform more.

CONCLUSION

A novel automated method for aneurysm growth quantification in longitudinal CTA data has been developed based on 4D groupwise registration. The 4D method agrees better with patient reports from clinical practice than individual 3D segmentation of each time point scan. Using the 4D method, apart from aneurysm growth, it is possible to measure local deformations of aneurysm wall and use this information in finding the potential regions of rupture. The developed method can benefit the clinical diagnosis and treatment planning in the sense that the results are objective and quantitative.

REFERENCES

1. Graves, E. J., "Detailed diagnoses and procedures, National Hospital Discharge Survey," Vital Health Stat. 13, 113-225 (1992).
2. Wermer, M. J., van der Schaaf, I. C., Velthuis, B. K., Majoie, C. B., Albrecht, K. W., Rinkel, G. J., "Yield of short-term follow-up CT/MR angiography for small aneurysms detected at screening, " Stroke. 37(2), 414-418 (2005).
3. Wermer, M. J., van der Schaaf, I. C., Velthuis, B. K., Algra, A., Buskens, E., Rinkel, G. J., "Follow-up screening after subarachnoid haemorrhage: frequency and determinants of new aneurysms and enlargement of existing aneurysms," Brain. 128(Pt 10), 2421-2419 (2005).
4. Dickey, P., Kailasnath, P., "The diameter-cube hypothesis: a new biophysical model of aneurysm rupture," Surg Neurol. 58(3-4), 166–173 (2002).
5. Chang, H. S., "Simulation of the natural history of cerebral aneurysms based on data from the International Study of Unruptured Intracranial Aneurysms," J Neurosurg. 104(2), 188–194 (2006).
6. Jou, L. D., Mawad, M. E., "Growth rate and rupture rate of unruptured intracranial aneurysms: a population approach," Biomed Eng Online. 18, 8-11 (2009).
7. Koffijberg, H., Buskens, E., Algra, A., Wermer, M. J., Rinkel, G. J., "Growth rates of intracranial aneurysms: exploring constancy," J Neurosurg. 109(2), 176-185 (2008).
8. Watton,, P. N., Ventikos, Y., Holzapfel, G. A., "Modeling the growth and stabilization of cerebral aneurysms," Math Med Biol. 26(2), 133-164 (2009).
9. Yoshimoto, Y., "A mathematical model of the natural history of intracranial aneurysms: quantification of the benefit of prophylactic treatment," J Neurosurg. 104(2), 195-200 (2006).
10. Burns, J. D., Huston, J. 3rd, Layton, K. F., Piepgras, D. G., Brown, R. D., Jr., "Intracranial aneurysm enlargement on serial magnetic resonance angiography: frequency and risk factors," Stroke. 40(2), 406-411 (2009).
11. Phan, T. G., Huston, J. 3rd, Brown, R. D., Jr., Wiebers, D. O., Piepgras, D. G., "Intracranial saccular aneurysm enlargement determined using serial magnetic resonance angiography," J Neurosurg. 97(5), 1023-1028 (2002).
12. Sprengers, M. E., van Rooij, W. J., Sluzewski, M., Rinkel, G. J., Velthuizen, B. K., de Kort, G. A., Majoie, C. B., "MR angiography follow-up 5 years after coiling: frequency of new aneurysms and enlargement of untreated aneurysms," AJNR Am J Neuroradiol. 30(2), 303-307 (2009).
13. Juvela, S., Poussa, K., Porras, M., "Factors affecting formation and growth of intracranial aneurysms: a long-term follow-up study," Stroke. 32(2), 485-491 (2001).
14. Firouzian, A., Manniesing, R., Flach, H. Z., Risselada, R., van Kooten, F., Sturkenboom, M. C. J., van der Lugt, A., Niessen, W. J., "Intracranial aneurysm segmentation in 3D CT angiography: Method and quantitative validation with and without prior noise filtering," Eur J Radiol. 79, 299-304 (2010).
15. Caselles, V., Kimmel, R., Sapiro, G., "Geodesic active contours," International Journal of Computer Vision. 22(1), 61-79 (1997).
16. Malladi, R., Sethian, J. A., "Image processing via level set curvature flow," Proc. Natl. Acad. Sci. USA. 92, 7046-7050 (1995).
17. http://www.vmtk.org

18. Ford, M. D., Hoi, Y., Piccinelli, M., Antiga, L., Steinman, D.A., "An objective approach to digital removal of saccular aneurysms: technique and applications," Br J Radiol. 82(Spec 1), S55-61(2009).

19. Cardenes, R., Pozo, J. M., Bogunovic, H., Larrabide I., Frangi, A. F., "Automatic aneurysm neck detection using surface Voronoi diagrams," IEEE Trans Med Imaging. 30(10), 1863-1876 (2011).

20. Metz, C. T., Klein, S., Schaap, M., van Walsum, T. and Niessen, W. J., "Nonrigid registration of dynamic medical imaging data using nD+t B-splines and a groupwise optimization approach," Medical Image Analysis. 15(2), 238-249 (2011).

21. Balci, S. K., Golland, P., Shenton, M., Wells, W. M., "Free-form B-spline deformation model for groupwise registration," Med Image Comput Comput Assist Interv. 10(WS), 23-30 (2007).

22. Bhatia, K. K., Hajnal, J., Hammers, A., Reuckert, D., "Similarity metrics for groupwise non-rigid registration," Med Image Comput Comput Assist Interv. 10(Pt 2), 544-552 (2007).

23. Klein, S., Staring, M., Murphy, K., Viergever, M. A., Pluim, J. P. W., "elastix: a toolbox for intensity-based medical image registration," IEEE Trans Med Imaging. 29(1), 196-205 (2010).

Chapter 5

Automated Quantification of Intracranial Aneurysm Growth in a Longitudinal CT Angiography Study

Chapter 6

Summary

Intracranial aneurysms are increasingly detected before rupture due to advances in non-invasive imaging technologies. The mechanisms through which aneurysms are formed or ruptured are mainly unknown. Some patients have a family history of aneurysmal rupture suggesting a genetic predisposition, while others have an underlying connective tissue disease. Incidental unruptured aneurysms have low risk of rupture, but in patients with a history of ruptured aneurysm, the risk is 10 times higher. Despite improvements in diagnosis and treatment of aneurysmal subarachnoid hemorrhage (SAH), its overall mortality rate remains high (40%-50%). Therefore, finding criteria for predicting aneurysm rupture is very important for therapeutic decision-making.

Advances in MR and CT technology have enabled the detailed, noninvasive assessment of the cerebral vasculature. In recent years, especially CT angiography (CTA) has become an important modality in the detection and management of intracranial aneurysms. It has almost replaced conventional digital subtraction angiography (DSA) for assessing presence and localization of intracranial aneurysms and in selecting the best treatment option. Compared to DSA, CTA is faster, has less risk for the patient, and enables a 3D visualization of cerebral vessels. This e.g. facilitates detailed surgical planning by the possibility to rotate and visualize the vasculature relative to other structures in the image. Furthermore, 4D CTA makes it possible to reconstruct multiple high resolution 3D images at different phases of the cardiac cycle, enabling the study of aneurysm morphodynamics.

In clinical practice, CTA scans of aneurysms are primarily analyzed visually. Performing manual quantitative assessment of intracranial aneurysms is quite challenging and includes interactions which are prone to inter- and intra-observer variability. Furthermore, manual analysis of 3D CTA data is time consuming. Low contrast, high noise levels, presence of imaging artifacts (e.g. from neighboring clips, windmill artifacts in 4D), surrounding anatomy with similar intensity characteristics, irregular aneurysm shape, and blooming effect are among the challenges that are encountered during manual assessment. Manual analysis of 4D CTA data for investigating aneurysm morphodynamics would be even more time consuming. Also, it would be prone to increased observer variability and error since the imaging data has a lower signal to noise ratio than the 3D case. Finally, assessment of aneurysm growth in longitudinal studies is highly challenging as growth may be subtle and images may have been acquired in different conditions. In view of these considerations, there is an urgent need for automated analysis for the objective extraction of aneurysm morphology, aneurysm morphodynamics and aneurysm growth.

In this thesis, we developed and evaluated automated tools to assist clinicians in performing faster, more accurate, reproducible and subjective assessments of intracranial aneurysm volume, growth and morphodynamics. These tools can extract more information from the imaging data than is manually feasible and address some of the challenges that are faced in manual assessment.

In **Chapter2** a semi-automated segmentation method was implemented using the level set frame work, more specifically Geodesic Active Surfaces. In this approach a surface is evolved to capture the aneurysmal wall via an energy minimization approach. The method was validated

against manual annotations of two observers. Since the results were in the range of the inter-observer variability, we conclude that the method has potential to replace the manual segmentation. Furthermore, in Chapter 2, the use of nonlinear diffusion filters (Gaussian filtering, RPM and EED) for image smoothing prior to segmentation was investigated. It was found that the segmentation accuracy slightly improved which has previously been shown for 3DRA as well when using edge-enhancing anisotropic diffusion filters. The method encountered problems in cases where the aneurysm and the surrounding vasculature were very close to the skull base. In such situations the segmentation may grow into the bone and manual interaction is required. In our study, this occurred in 25% of the cases.

In **Chapter 3**, a method to investigate the dynamic behavior of intracranial aneurysms from ECG-gated CTA data was developed and evaluated. Previous studies on intracranial vasculature dynamics used thresholding and manual interactions for visualizing and quantifying vascular deformation. However, considering the low resolution, noise, and small size of aneurysms, accurate segmentation and volume measurements in dynamic data is challenging when relying only on intensity values in each phase. Therefore, we opted for a method which can take into account the possible variations of intensity in different phases of the time series, artifacts and patient motion. The method consists of two steps: registration of the multiphase 3D (4D) data to acquire the deformation field which describes the local deformation of image structures in all phases, and aneurysm segmentation (see Chapter2). In the absence of a ground truth, the method was validated against simulated 4D deformations. The results indicated that the proposed method is capable of quantifying intracranial aneurysm volume changes and visualizing local aneurysmal wall motion from ECG-gated CTA during a heart cycle. This provides additional information on the status of the aneurysmal wall which, together with other geometrical information, may help to better estimate aneurysm growth and predict rupture risk. For validation purposes, the dynamics of a healthy vessel segment and part of the skull were analyzed using the same method and the results were compared to the estimated aneurysmal wall motion. Since the aneurysm wall has different properties than a healthy vessel segment, it is expected that aneurysms have larger volume changes over the cardiac cycle which was indeed observed. Also, as expected, no significant volume change in the bone area was observed, suggesting that the reported changes are due to actual aneurysmal wall motion and not due to image reconstruction errors, patient motion, noise, or other artifacts. Whereas the results show that aneurysm motion can be investigated using this automated analysis method, further research in a prospective setting is required to determine the additional value of aneurysm morphodynamics in the context of predicting aneurysm growth and estimating rupture risk.

Aneurysm growth over time is another important indicator for aneurysm rupture risk. In **Chapter 4,** two automated approaches have been proposed and investigated for quantifying aneurysm growth in CTA data acquired in a longitudinal study. One method treats a longitudinal series of images as a time series image (stack of 3D images), and utilizes 4D groupwise registration, in combination with aneurysm segmentation of the first time point scan, to determine aneurysm growth. The other method is based on the application of a 3D segmentation method,

previously presented in Chapter 2, to each time point individually. The results show that the 4D approach agrees better with patient reports from clinical practice than individual 3D segmentations at each time point. In addition to assessing aneurysm growth, the 4D method can also measure local deformation of the aneurysm wall.

Having developed an automated method for aneurysm growth quantification in a longitudinal study (Chapter 4), the method was applied to larger number of CTA data to further investigate possible associations of aneurysm growth with size, location, age and sex (**Chapter 5**). The results show that the growth rate per year was largest at PCoA and was not statically significant difference between male and female patients. There were no clear associations found between growth rate and size and age. The measurements performed by the method were compared to manual assessment as well. The method had a better agreement with the consensus than the observers with each other. However, the evaluation by comparison with manual measurements was hampered by the fact that most of the aneurysms did not grow and there was considerable disagreement between observers. Image artifacts and image quality played a large role in the observed variability. Reviewing the results showed that the disagreement between the observers was caused either because the aneurysm was slightly displaced in the follow-up scan or due to the presence of thrombus. The disagreement between the method and the consensus was influenced by large difference in contrast between scans or the presence of imaging artifacts which were not overcome by the method completely.

In conclusion, whereas automated aneurysm volume assessment has received some attention in the last years, automated methods for quantifying intracranial aneurysms dynamic behavior and aneurysm growth in longitudinal studies, as developed in this thesis, are novel. Since both aneurysm motion and aneurysm growth are often very subtle, measurements need to be performed very accurately. In most cases, the naked eye is not able to assess such changes reliably, and thus there is room for automated methods to play an important role. The evaluations carried out in this thesis show that the methods developed here can play such role. However, we have to note that a more thorough evaluation in prospective longitudinal studies is required to assess the real value of these measures in predicting growth and estimating rupture risk. Results of such studies will provide insight into the value of these tools in the management of patients with aneurysms.

It is our strong belief that automated methods in the assessment of intracranial aneurysms will increasingly be used in clinical practice. First, it will make the diagnostic process faster, more objective, reproducible, and potentially more accurate. Second, it may lead to more personalized treatment planning. In addition to the methods developed in this thesis, there are other possible image analysis methods to support in the diagnosis and treatment planning of patients with aneurysms. For example, there is interest in techniques for automated aneurysm detection, for use in a screening situation. Currently, when visually inspecting a dataset, newly formed aneurysms can be missed because of their small size or being close to the skull base. With computer assistance, the chances of this happening can potentially be reduced.

SAMENVATTING

Dankzij ontwikkelingen in niet-invasieve beeldvormende technieken worden er steeds meer intacte aneurysma's in de hersenen (intracraniële aneurysma's) gevonden. Het is grotendeels onduidelijk hoe aneurysma's ontstaan en waardoor ze kunnen scheuren en een hersenbloeding veroorzaken. Er zijn aanwijzingen voor een erfelijke component aangezien in sommige families rupturen relatief vaak voorkomen. In andere patiënten is er sprake van een onderliggende aandoening aan het bindweefsel. Intacte intracraniële aneurysma's die bij toeval worden ontdekt, hebben een laag risico op scheuren, maar deze kans is wel 10 keer zo groot in patiënten met een eerdere ruptuur. Ondanks verbeteringen in de diagnose en behandeling van hersenbloedingen is de kans op overlijden nog altijd groot (40%-50%). Het vinden van nieuwe criteria voor het voorspellen van een ruptuur is daarom van groot belang.

Door de ontwikkelingen in CT en MR is het tegenwoordig mogelijk om het vaatstelsel in het hoofd goed te beoordelen. Met name CT angiografie (CTA) is belangrijk geworden voor het detecteren en opvolgen van intracraniële aneurysma's. Bij het vinden, localiseren en het kiezen van een behandelingsmethode van aneurysma's heeft deze modaliteit digitale subtractie angiografie (DSA) grotendeels vervangen. CTA is sneller en minder risicovol voor de patiënt dan DSA, en het is bovendien mogelijk om een 3D visualisatie te maken. Dit biedt de mogelijkheid het vaatstelsel te roteren en af te beelden ten opzichte van de omliggende structuren, wat het plannen van een ingreep makkelijker maakt. Daarnaast kan de radioloog met behulp van een 4D CTA een reconstructie maken van opeenvolgende hoge resolutie 3D scans, om daarmee de vervorming van het aneurysma tijdens de hartcyclus te bekijken.

In de kliniek worden CTA scans van aneurysma's meestal visueel beoordeeld. Handmatige kwantitatieve analyse van intracraniële aneurysma's is moeilijk en tijdrovend en de resultaten vertonen *inter-* en *intra-observer* variabiliteit. Lage contrasten, hoge ruisniveaus, artefacten (b.v. van clips, of *windmill* artefacten in 4D), nabijgelegen structuren met dezelfde intensiteitskarakteristieken, de soms grillige vorm van het aneurysma en *blooming* zijn een aantal problemen die dit proces bemoeilijken. Manuele analyse van de morfodynamica in 4D CTA data kost nog meer tijd dan in 3D data, en is daarnaast gevoeliger voor fouten vanwege de slechtere signaal-ruisverhouding. Tenslotte is het handmatig meten van de ontwikkeling van aneurysma's in longitudinale beelddata zeer moeilijk vanwege de vaak trage groei, zeker als de scans onder verschillende omstandigheden zijn gemaakt. Al met al bestaat er daarom een grote behoefte aan automatische methodes om het volume, de vervorming, en groei van aneurysma's objectief te meten.

In dit proefschrift hebben we automatische technieken ontwikkeld en geëvalueerd om clinici te ondersteunen bij het sneller en nauwkeuriger meten van het volume, de groei en vervorming van intracraniële aneurysma's op een reproduceerbare en objectieve wijze. Deze technieken bieden een oplossing voor een aantal van de problemen van handmatige metingen en kunnen daarnaast ook meer informatie extraheren uit de beelddata.

In **Hoofdstuk 2** is een semi-automatische segmentatiemethode geïntroduceerd op basis van *Geodesic Active Surfaces level sets*. In deze techniek wordt een 3D oppervlakte geëvolueerd op basis van energie minimalisatie met als doel het vinden van de aneurysmawand. De methode is gevalideerd met behulp van manuele segmentaties door twee clinici. Omdat de nauwkeurigheid van de automatische methode vergelijkbaar was met die van de clinici onderling concluderen we dat deze methode als vervanging zou kunnen dienen van manuele segmentatie. Daarnaast werd ook het nut onderzocht van het vooraf filteren van de beelddata met niet-lineare diffusiefilters (Gaussische filters, RPM en EED). De nauwkeurigheid van de segmentatie werd iets groter na toepassing van een *edge-enhancing anisotropic diffusion filter*, een resultaat dat eerder ook werd gevonden voor 3D RA beelden [5]. De segmentatiemethode had de meeste problemen in gevallen waar het aneurysma of aangrenzende vaten zich dicht bij de schedelbasis bevonden. De level set kan dan het bot ingroeien waardoor een manuele correctie nodig is. Tijdens deze studie trad dit probleem op in 25% van de gevallen.

In **Hoofdstuk 3** is een methode ontwikkeld en geëvalueerd om het dynamisch gedrag van aneurysma's in *ECG-gated* CTA beelden te analyseren. Eerdere studies naar de dynamica van intracraniële vaten gebruikten drempeling en manuele interactie om deformaties te visualiseren en kwantificeren. Maar segmentatie van dynamische data op basis van intensiteitswaardes alleen is moeilijk vanwege de lage resolutie, ruis en de geringe afmetingen van aneurysma's. Vandaar dat we hebben gekozen voor een methode die rekening houdt met intensiteitsvariaties gedurende de hartcyclus, beeldartefacten en beweging van de patiënt. De methode bestaat uit twee stappen: eerst wordt een bewegingsveld bepaald door registratie van de multi-fase 3D (4D) data. Dit bewegingsveld beschrijft de lokale vervorming van het beeld gedurende de hartcyclus. Deze stap wordt gevolgd door segmentatie van het aneurysma (zie Hoofdstuk 2). Bij gebrek aan een gouden standaard werd de methode gevalideerd met behulp van gesimuleerde 4D deformaties. Uit deze vergelijking bleek dat de methode in staat is om op basis van ECG-gated CTA beelden volumeveranderingen te meten en de lokale vervorming van het aneurysma tijdens de hartslag te visualiseren. Deze methode geeft dus nieuwe mogelijkheden om de conditie van het aneurysma te karakteriseren, wat samen met andere geometrische informatie kan worden gebruikt om de groei en risico op een ruptuur te schatten. Als extra validatie werd de methode ook toegepast op een gezond vat en een deel van het schedelbot. Deze resultaten werden vergeleken met de gemeten beweging van de aneurysmawand. Zoals verwacht vertoonde de aneurysmawand grotere volumeverschillen dan het gezonde vat. In het bot werden geen significante volumeveranderingen gemeten; de metingen in het aneurysma lijken dus niet veroorzaakt door reconstructiefouten, beweging van de patiënt, ruis of andere artefacten. Deze resultaten tonen aan dat de in dit proefschrift beschreven methode de vervorming van aneurysma's kan analyseren. Of deze vervorming toegevoegde waarde heeft in het voorspellen van groei of ruptuur zal onderzocht moeten worden in een prospectieve studie.

Een andere belangrijke indicator voor het risico op scheuren is de groei van een aneurysma. In **Hoofdstuk 4** worden twee automatische methodes geïntroduceerd die de groei kunnen meten in longitudinale CTA beelddata. In de eerste methode worden de opeenvolgende 3D volumes beschouwd als een 4D beeld. Met behulp van 4D groepsgewijze registratie, in combinatie met een segmentatie van het eerste tijdspunt, kan dan de groei van het aneurysma worden gemeten. In de tweede methode worden de opeenvolgende 3D volumes onafhankelijk van elkaar gesegmenteerd met de techniek uit Hoofdstuk 2. De resultaten van de 4D aanpak bleken beter overeen te komen met verslagen uit de kliniek dan bij het apart uitvoeren van de 3D segmentaties. Daarnaast kan de 4D methode ook de lokale vervorming van de aneurysmawand meten.

De automatische methode voor groeimeting in longitudinale beelddata uit Hoofdstuk 4 werd vervolgens toegepast op een groot aantal CTA scans om de associaties te onderzoeken tussen de groei van een aneurysma aan de ene kant, en aneurysmagrootte, sekse en leeftijd aan de andere kant (**Hoofdstuk 5**). De resultaten lieten zien dat de groeisnelheid het hoogste was in de posterior communicating artery en er geen statistisch significant verschil is tussen mannen en vrouwen. Tussen grootte of leeftijd en groei werden geen associaties gevonden. Deze automatische metingen werden ook vergeleken met handmatige metingen. De automatische resultaten kwamen beter overeen met de handmatige consensusmeting dan de handmatige metingen met elkaar. Een beperkende factor bij deze vergelijking was het feit dat de meeste aneurysma's niet groeiden, en de metingen van beide clinici erg veel van elkaar verschilden. Artefacten en beeldkwaliteit speelden hierbij een grote rol. Inspectie van alle resultaten toonde aan dat de verschillen in handmatige segmentatie werden veroorzaakt door een kleine verschuiving in de tweede scan of door een trombus. Verschillen tussen de manuele en automatische metingen werden vooral veroorzaakt door grote contrastverschillen tussen de twee opeenvolgende CTA scans of grote artefacten die de resultaten van de automatische methode negatief beïnvloedden.

Hoewel volumemetingen van aneurysma's de afgelopen jaren veel aandacht hebben gekregen, zijn de automatische methodes om vervorming en groei van aneurysma's te meten, zoals beschreven in dit proefschrift, een nieuwe ontwikkeling. De subtiele beweging en groei van aneurysma's stellen hoge eisen aan de nauwkeurigheid van de metingen. In veel gevallen is het blote oog niet in staat om deze veranderingen op te merken en is er dus een rol weggelegd voor automatische metingen. De evaluaties in dit proefschrift tonen aan dat automatische methodes ook inderdaad in staat zijn om deze rol te vervullen. Wel zijn er prospectieve studies met longitudinale beeldvorming noodzakelijk om de voorspellende waarde te onderzoeken van deze metingen voor groei of risico op ruptuur. Dergelijke studies zullen inzicht geven in de klinische waarde van de ontwikkelde methodes.

We zijn er van overtuigd dat automatische methodes voor de beoordeling van intracraniële aneurysma's steeds meer gebruikt zullen worden in de kliniek. Ze kunnen de diagnose versnellen, objectiever en reproduceerbaarder maken, en mogelijk ook nauwkeuriger. Daarnaast

zouden dergelijke technieken een bijdrage kunnen leveren aan individuele behandeltrajecten. Naast de methodes uit dit proefschrift zou beeldanalyse ook andere bijdragen kunnen leveren aan de diagnose en behandeling van aneurysma's. Zo is er een behoefte aan technieken voor het automatisch detecteren van de eventuele aanwezigheid van een aneurysma voor screening. Momenteel kunnen pas gevormde aneurysma's over het hoofd worden gezien vanwege hun beperkte grootte of nabijheid bij de schedelbasis. Computers kunnen mogelijk de kans hierop verkleinen.

PUBLICATIONS

Journal Papers

Firouzian A, Manniesing R, Metz CT, Bor ASE, Klein S, Velthuis BK, Rinkel GJE, van der Lugt A, Niessen WJ. Automated quantification of intracranial aneurysm growth in a longitudinal CT angiography study, submitted.

Firouzian A, Manniesing R, Metz CT, Risselada R, Klein S, van Kooten F, Sturkenboom MCJM, van der Lugt A, Niessen WJ. Quantification of intracranial aneurysm morphodynamics from ECG-gated CT angiography, Acad Radiol 2012; in press.

Risselada R, de Vries LM, Dipple DW, van Kooten , van der Lugt A, Niessen WJ, **Firouzian A**, Stricker BH, Sturkenboom MC. Incidence, treatment and case-fatality of non-traumatic subarachnoid haemorrhage in the Netherlands, Clin Neurol Neurosurg 2011; 113(6):483-487.

Risselada R, Straatman H, van Kooten F, Dippel DW, van der Lugt A, Niessen WJ, **Firouzian A**, Herings RM, Sturkenboom MC. Platelet aggregation inhibitors, vitamin K antagonists and risk of subarachnoid hemorrhage, J Thromb Haemost 2011; 9(3):517-523.

Firouzian A, Manniesing R, Flach ZH, Risselada R, van Kooten F, Sturkenboom MC, van der Lugt A, Niessen WJ. Intracranial aneurysm segmentation in 3D CT angiography: Method and quantitative validation with and without prior noise filtering, Eur J Radiol 2011; 79(2):299-304.

Risselada R, Straatman H, van Kooten F, Dippel DW, van der Lugt A, Niessen WJ, **Firouzian A**, Herings RM, Sturkenboom MC. Withdrawal of statins and risk of subarachnoid hemorrhage, Stroke 2009; 40(8):2887-2892.

Conference Papers

Firouzian A, Manniesing R, Metz CT, Klein S, Velthuis BK, Rinkel GJE, van der Lugt A, Niessen WJ. Intracranial aneurysm growth quantification in CTA, SPIE Medical Imaging 2012; Proc. of SPIE 8314, 831448.

Firouzian A, Manniesing R, Flach HZ, Risselada R, van Kooten F, Sturkenboom MC, van der Lugt A, Niessen WJ. Intracranial aneurysm segmentation in 3D CT angiography: method and quantitative validation, SPIE Medical Imaging 2010; Proc. of SPIE 7623, 76233M.

Firouzian A, Manniesing R, Flach HZ, Risselada R, van Kooten F, Sturkenboom MC, van der Lugt A, Niessen WJ. Intracranial aneurysm segmentation in 3D CT angiography: method and quantitative validation, Radiological Society of North America, 94th Scientific Assembly and Annual Meeting, 2008.

ACKNOWLEDGEMENTS

This is such a pleasurable moment to sit on top of the mountain, look down at the bottom and see how far you came up and how much you have learned on the way. When I think about it, I cannot believe the amount of knowledge I gained during the last few years. I remember the very first day at BIGR, I began reading Milan Sonka's book from definition of an image. Now I even receive papers to review. To be honest I feel very proud of myself but of course this would not be possible without all the support and help I got from my supervisors, colleagues, friends and family. This is the moment to thank them all for what they have done for me during this period.

First and foremost, I would like to express my sincere gratitude to my promotor, Prof. dr. Wiro Niessen. Dear Wiro, working with you was a real pleasure. Your insight, supervision and guidance were invaluable to me. You gave me the opportunity to be part of BIGR and led me through my PhD trajectory till the very last moment. I learned a lot from you. You were there for me, despite your busy agenda, whenever I needed your advice on both research and personal matters. I was very lucky to have you as my promotor.

I would also like to acknowledge my co-promotor, Dr. ir. Rashindra Manniesing. Dear Rashindra, I benefited from your advices, triggering ideas and programming skills. You were following this project enthusiastically and encouraging me in moments of despair. I appreciate your dedication to research and willingness to share your knowledge and expertise.

Furthermore, a very special thanks goes to my medical supervisor, Prof. dr. Aad van der Lugt. Dear Aad, thank you for teaching me all about the brain vasculature and sharing your medical knowledge and expertise throughout my PhD trajectory. I appreciate your passion for research and cooperation despite your busy schedule and dank dat u mij aanmoedigde om Nederlands te leren.

I am grateful to the committee members for accepting the invitation to be part of the doctoral committee and making the effort and time to read this thesis.

Chapter 2 and 3 were performed as part of the @aneurist project which was a European project. I would like to use this opportunity to thank all the CISTIB lab colleagues in Pompeu Fabra University, Barcelona, who were hosting the project meetings. I enjoyed very much spending time, brainstorming, exchanging ideas and socializing with you. On top of that you helped me to learn more about the Spanish culture, food and habits. These trips were among the best business trips that I went on. On these trips, I had the pleasure to be with two other colleagues from Erasmus MC, IPCI group: Dr. R. Risselada and Prof. Dr. M.C. Sturkenboom. Dear Miriam, it was an honor for me to work with you on the same project and accompany you in the meetings. Thank you for being there for me, caring about me and sharing your experiences with me whenever I was getting off the track. Dear Roelof, my colleague and friend, I very much enjoyed working and discussing with you. Thank you for being so responsible, friendly and concerned. I miss the fruitful coffee break chats. Furthermore, I would like to thank Dr. Fop van Kooten for recruiting

patients, Dr. Zwenneke Flach for participating in the manual evaluation, Marcel Dijkshoorn for scanning the patients, Dr. Marcel van Straaten for performing the phantom scanning in this study.

In chapter 4 and 5 of this thesis, we collaborated with UMC Utrecht and used their data for our study. I would like to express my appreciation to Prof. dr. G.J.E. Rinkel, Dr. B.K. Velthuis and Dr. A.S.E. Bor for sharing their data, especially Dr. Bor who participated in manual evaluation of the results as well. I also got the opportunity to work more closely with Dr. ir. Stefan Klein and Dr. Coert Metz. Dear Stefan and Coert, thank you for your brilliant ideas, being cooperative and sharing your knowledge with me.

I would like to express my appreciation to colleagues who were not directly involved in the project but were always supporting me with their ideas and skills. Ir. R. Hameeteman, dear Reinhard, the MeVisLab master, thank you for patiently answering all my stupid questions about MeVisLab and never being fed up. Dr. ir. F. van der Lijn, dear Fedde, thank you for all the honest and direct opinions, advises and discussions. You were always offering me your support and always had time for me. The live evidence is translating my thesis summary to Dutch for which I am grateful to you. Dr. ir. E. Meijering, dear Erik , it was a great pleasure for me to have philosophical discussions with you in the coffee breaks. I was always inspired by your point of view and approach to life. Dr. M. Rentmeester, dear Mart, thank you for all your software support and being responsive to unexpected problems.

It is always desired to have nice company and share your pain when you are struggling with a project and trying to get some results. Indeed that was the case for me and I am thankful to my office mates (Reinhard Hameeteman, Karin Bol, Gerardo Dibildox, Coert Metz, Maruis de Groot) for creating a peaceful and work-friendly environment. It is also desired to have some social life next to your work and again that was the case for me. I spent a lot of memorable time with my colleague friends (Rahil Shahzad, Hortense Kirisli, Nora Baka, Noemi Carranza, Silvana Romio, Ana Afonso). Social life in Rotterdam would be very tough without you. In BIGR, thanks to Wiro, we also had several outings every year. I am thankful to all BIGR colleagues for making the outings unique and unforgettable experiences.

In a young and fast growing group such as BIGR, it is not easy to arrange meetings, appointments, seminars, the paper work, etc. Luckily, these were all managed by Ms. P. Assems and Ms. D. De Jong. Dear Petra, thank you for having a smiling face all the time, being responsible, arranging progress meetings with Wiro despite his hopelessly busy schedule. Dear Desiree, thank you for arranging the administrative work during this period specially the last few months.

Among all the stress factors that I was dealing with over the last few years was my visa issue which needed a lot of administrative work and bureaucracy. But fortunately Ms. S. Degenaar and Mr. A. Engelhard, from P&O office, were there to help me. Dear Solange and Andreas, thank you for helping me with all the hassle that I had to go through because of IND and the others.

Ik wil graag mijn leraren Nederlands, Stella Maaswinkel en Ellis Delken, bedanken. Beste Stella en Ellis, dank dat jullie mij de mogelijheid gaven om de cursus te volgen. Jullie hebben

mij veel gesteund en gemotiveerd om Nederlands te leren tijdens mijn promotie periode en mijn diploma Nederlands als tweede taal te halen.

My dear friends, Behnaz Pourebrahimi, Jawad Qureshi, Raha Pazoki & Abbas Dehghan, Kamana Sigdel, Sepideh Babaei, Tahmineh Fadaei & Alireza Mohseni, Yousef Ebrahimi, Gerrie & Martin van den Enden, Parisa Yousefdoust, Maryam Hashemi, Mohammad Taleghani, Leila Mohammadi, Setareh Jafari, Helena Raulus, Marzieh Haddadian , Saba Sanadgol, Soheila Fallahi, Saeed & Hengameh Fallahi, Leili & Behzad Saadati, Nikta Amiri, Zohreh Jafari, Behesht Fakhraee, Borzoo Nabet, Vahdat Rashidi, Nasrin Esfandiari, Mina Danesh, Sahar Esteghamat, Yaser Atlasi, Babak Ghafari and mijn lieve buren, Hans en Corrie Brouwer. Thank you for making this tough period of my life more pleasant. I could not do this without your moral support. I am also thankful to my friends and relatives in Iran and the rest of the world who always send their warm regards and support from far, Parish Forouzesh, Nazanin Fatemi, Parvaneh Farhady, Roghyeh Sadeghzadeh, Pegah Fatemi, Neda Ghasemi, Mehdi Nouri, Ali Jahandideh, Ali Pashaei, Mehdi & Maryam Nouri, Esmaeil Nadimi, Rahim & Shideh Malekshahi, Hamid Esmailzadeh, Ali & Zahra Barati, Habib Valiollahi, Abbas Haddadi, Azadeh & Omid Noroozian, my beloved cousin (Dr. Nima Sattari) and my lovely uncle (Dr. Rahim Sattari).

Last but not least, very special thanks go to my dearest parents and my sweet little sister, Sepideh. Whatever I have and whoever I become is because of you. Without your unconditional love and support in all aspects, I would not be able to make it happen. I am very blessed to have you by my side.

درپایان ، نوبت میرسد به تقدیر و تشکر از عزیزترین ها، پدر و مادر و خواهرم سپیده. بابا ، مامان و سپیده عزیزم ، نهایت سپاس و تشکر را ازشما دارم که با محبت بی دریغتان در این مدت من را یاری کردید. زبان من از تشکر قاصراست که هر چه دارم و هر که هستم از شماست. بدون کمک و مهر بی پایان شما رفتن این راه برای من امکان پذیر نبود. من بسیار خوشبخت و خرسندم که شما را در کنار خود دارم .

Azadeh Firouzian
December 2012

PHD PORTFOLIO

Departments: Radiology and Medical Informatics, Erasmus MC Rotterdam
Research schools: ASCI and COEUR

	ECTS*	Year
Courses		
Knowledge driven image segmentation	4	2007
Front-end vision and multi-scale image analysis	4	2007
Advanced pattern recognition	4	2008
Peripheral and intracranial aneurysmal disease	1.5	2008
IEEE EMBS international summer school, Berder, France	3	2008
Molecular biology in cardiovascular research	1.5	2009
Scientific writing in English for publication	2	2010
Introduction to SPSS	1.5	2010
Speaking in public	1	2011
Presentations at international conferences		
RSNA, Chicago, USA	1	2008
SPIE Medical Imaging, San Diego, USA	1	2010
SPIE Medical Imaging, San Diego, USA	1	2012
Attending international conferences		
RSNA, Chicago, USA	1.8	2008
SPIE Medical Imaging, San Diego, USA	1.8	2010
ISBI, Rotterdam, the Netherlands	1.2	2010
SPIE Medical Imaging, San Diego, USA	1.8	2012
Presentations at national conferences, symposia and seminars		
Research seminars at BIGR	4	2007-2012
Research Colloquia at department of Medical Informatics	2.4	2007-2012
Research seminars at department of Radiology	1.6	2007-2012
Journal club at BIGR	1.6	2007-2012
Medical informatics days, Renesse	0.8	2008
North Sea neurovascular network	0.8	2012
COEUR course on atherosclerotic and aneurysmal disease	0.8	2012
Research seminar at DIAG, UMC St. Radboud Nijmegen	0.8	2012
Research seminar at BME group, EMC Rotterdam	0.8	2012

Attending national conferences, symposia and seminars

Dutch BME Conference, Egmond aan Zee, the Netherlands	0.6	2007
Research seminars at BIGR	1	2007-2012
Research Colloquia at department of Medical Informatics	1	2007-2012
Research seminars at department of Radiology	1	2007-2012
Journal club at BIGR	1	2007-2012
Medical informatics days, Nijmegen	0.6	2007
Medical Imaging Symposium for PhD students, Utrecht	0.3	2007
Medical informatics days, Renesse	0.6	2008
Netherlands Forum for Biomedical Imaging, Delft	0.3	2008
Medical Imaging Symposium for PhD students, Leiden	0.3	2008
Medical Imaging Symposium for PhD students, Delft	0.3	2009
Total	**52.7**	

Professional memberships

IEEE, EMBS

Peer reviews

IEEE transactions on Medical Imaging

* European Credit Transfer System; 1 ECTS = 28 hours of study.

ABOUT THE AUTHOR

Azadeh Firouzian was born in March 1979 in Tehran, Iran. She finished her high school there and entered university. She got her BSc in Biomedical Engineering from Shahid Beheshti University of Medical Sciences (Tehran, Iran) in 2002 and her bachelor's thesis was on designing "A Novel Model for Purchasing Medical Instrumentation". Then she decided to go abroad, explore the world, face new challenges and continue her educations. In 2003, she entered HAN University (Hogeschool van Arnhem en Nijmegen) and studied Master in Control System Engineering for half a year. In January 2004, she got admission to TU Delft and in April 2006, she got her MSc in Biomedical Engineering with a specialization in Instrumentations and Sensors. Her master's thesis was on designing "Integrated Electrodes for Blood Impedance Measurements". Her curiosity and passion for knowledge did not let her stop education. Therefore, in December 2006, she joined BIGR to perform her PhD research on "Automated Analysis of Intracranial Aneurysm Morphology and Dynamics from CTA Data". It was part of a European project called @neurist with more than 20 collaborators. She enjoyed working on this project and published a number of articles in international journals and conferences.